Pyrite Biomineralization and Arsenic Sequestration at a Florida Industrial Site: Imaging and Geochemical Analysis

by

Theodore Jeffrey Wilson

A thesis submitted to the Graduate Faculty of
Auburn University
in partial fulfillment of the
requirements for the Degree of
Master of Science

Auburn, Alabama
May 5, 2018

Keywords: arsenic, bioremediation, biomineralization, geochemistry, imaging, groundwater

Approved by

Ming-Kuo Lee, Chair, Robert B. Cook Professor of Geology
James A. Saunders, Professor Emeritus of Geology
Ashraf Uddin, Professor of Geology

Abstract

A yearlong field-scale bioremediation experiment was conducted at a Florida industrial site, where groundwater in an unconfined aquifer was contaminated by an arsenic-based herbicide. The bioremediation technique stimulated the indigenous sulfate reducing bacteria (SRB) with a nutrient-rich slurry solution containing labile organic carbon, ferrous iron, sulfate, and fertilizer. This amendment induced sulfate reducing conditions and caused the co-precipitation and adsorption of the dissolved arsenic in biogenic pyrite. This research characterized the biogenic pyrite formed and assessed the spatial and temporal changes in groundwater chemistry during the project. Pyrite was characterized using multiple techniques including X-ray diffraction, X-ray fluorescence, scanning electron microscopy, and electron microprobe analysis. These analyses confirmed the rapid formation of pyrite one week after the injection. The pyrite formed either as well-defined euhedral nano-crystals or as spherical aggregates (framboids) 1-50 μm in diameter. The electron microprobe analysis determined that the pyrite contained between 0.05-0.4 weight % of sequestered arsenic. The dissolved arsenic concentration in the water decreased from pre-injection levels of 300-500 ppb to below the site regulatory limit of 50 ppb (> 90% removal rate) during the initial six month period. The reactive transport of the injectant plume was investigated using a conservative chloride tracer and biomineralization of pyrite along two flow transects. The results show that the stimulated pyrite biomineralization accounted for more than 80% of overall arsenic removal and dilution caused less than 20% of concentration reduction. Saturation index calculations show that arsenian-pyrite

quickly became oversaturated in targeted wells one week after injection of the solution and then remained mostly saturated during the one-year monitoring period, suggesting that the arsenic sequestration was effectively maintained by the stability of arsenian-pyrite. This research presents data showing through the amendment of a nutrient-rich solution, indigenous SBR can effectively sequester arsenic into pyrite at levels great enough to bring dissolved arsenic concentrations below the regulatory or perhaps even drinking water standards.

Acknowledgments

Grants obtained from the National Science Foundation were integral to the execution of this research. I would like to thank the following people who generously gave their time, advice, and criticisms: Dr. Ming-Kuo Lee, Dr. James Saunders, Dr. Ashraf Uddin, and the entire faculty at the Auburn Department of Geosciences. A special thanks to the chair of my advising committee, Dr. Lee, who provided me with invaluable guidance and mentorship during my time at Auburn. He always had an open door and was more than willing to help with any problem or question I encountered. A thanks is also owed to Dr. Saunders for his guidance and hand in recruiting me to Auburn University. Another member of the Geosciences Department that was vital to my research was Dr. Billor. He provided me with strong support during the laboratory analysis portion of my thesis and taught me many lessons on laboratory procedure. I would also like to thank Dr. Hames and Dr. Brueckner for their help with my electron microprobe analysis and Dr. Miller of the Department of Biological Sciences for his help training me to use the scanning electron microscope. A special thanks to Dr. Jim Redwine, Justin Marks, Brett Surles, and Rick Hagendorfer, who helped to facilitate the injection process and field sampling, as well as data collection. I would like to thank Eric Levitt for being a mentor of mine and helping with sample collection. Lastly, I would like to thank all the friends I've made in Auburn during my time here and my family for their constant support.

Table of Contents

List of Tables

List of Figures

List of Abbreviations

As	Arsenic
Ca	Calcium
Cl	Chlorine
DO	dissolved oxygen
Eh	Redox potential
EPA	Environmental Protection Agency
EMP	Electron microprobe
FDEP	Florida Department of Environmental Protection
Fe	Iron
GWB	Geochemist's Workbench
GIS	Geographic Information System
H_2S	Hydrogen Sulfide
IC	Ion chromatograph
ICP-MS	Inductively Coupled Plasma Mass Spectroscopy
K	Potassium
MCL	Maximum Contaminant Level
Mg	Magnesium
Na	Sodium
ORP	Oxidation-Reduction Potential

Ppb	Parts per billion
Ppm	Parts per million
Rpm	Rotations per minute
SEM	Scanning Electron Microscope
SO_4	Sulfate
SRB	Sulfate Reducing Bacteria
XRD	X-Ray Diffraction
XRF	X-Ray Fluorescence
WDS	Wavelength dispersive spectrometers

Introduction

Arsenic groundwater contamination poses a vast threat to the availability of safe and clean drinking water for a large portion of the world's population, especially in South Asia. In the United States, the Environmental Protection Agency (EPA) has grown increasingly concerned with arsenic contamination of drinking water, as evidenced by the recent revision to the arsenic drinking water standard, from 50 parts per billion (ppb) to 10 ppb (USEPA, 2001). Arsenic is also considered as the second-most common contaminant of concern at superfund sites in the United States (USEPA, 2002). The need to recognize and manage this common form of contamination has spurred a great deal of research to understand arsenic biogeochemical cycling in groundwater environments and to establish viable remediation techniques (Zouboulis et al., 1993; Bulut et al., 2000; Jingtai and Fyfe).

Both natural and anthropogenic sources of arsenic contribute significantly to groundwater contamination. Naturally occurring arsenic is relatively abundant in crustal rocks, with an average concentration of 10 parts per million (ppm) (Smedley and Kinniburgh, 2002). Alluvial aquifers, black shales, and hydrothermal systems have been shown to contain more elevated levels of arsenic than most other natural environments (Nordstrom, 2002). As proposed by Saunders et al. (2005a) the main driving mechanism behind the natural enrichment of arsenic in alluvial aquifers is a combination of mechanical weathering associated with glaciations, transport and adsorption of arsenic in stream sediments, and the subsequent deposition in alluvial deposits. Depending on the redox state of these alluvial aquifers, arsenic can either be mobile or immobile, which consequently has a vast impact on the extent of contamination. This source of natural arsenic contamination is common in south Asian countries such as Bangladesh and India (Kinniburgh and Smedley, 2001; Mandal and Suzuki, 2002; Nordstrom, 2002).

Anthropogenic sources of arsenic are 3 times more common than natural sources (Woolson, 1983). This is due to the heavy use of arsenic in the mid-20th century in the manufacturing of agricultural products, such as insecticides and herbicides, as well as the high arsenic concentrations in mine tailings (USEPA, 1997; Mandal and Suzuki, 2002). Therefore, anthropogenic sourced arsenic contamination is much more common in industrialized countries such as the United States. This widespread global problem with arsenic contamination (Figure 1) has led to an abundance of research pertaining to arsenic geochemistry and cycling especially in low temperature geochemical settings.

Arsenic-contaminated groundwater can be remediated using one of two general approaches, ex-situ or in-situ. Ex-situ techniques such as pump-and-treat or soil removal have been shown to be expensive and less effective than in-situ techniques such as permeable reactive barriers or bioremediation (Lee et al., 2000; Ford et al., 2007). Bioremediation using sulfate reducing bacteria (SRB) has been shown to be an economical and effective method of remediation as the constituents needed to activate the SRB are inexpensive and environmentally friendly (Saunders et al., 2008).

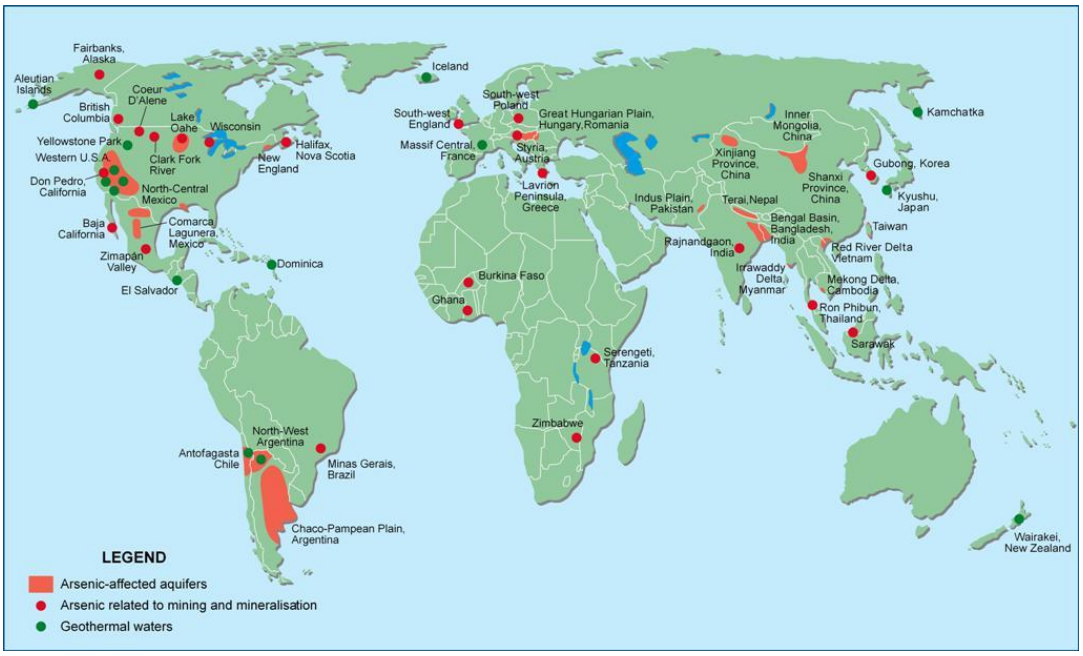

Figure 1. World map showing the distribution of arsenic groundwater contamination from both anthropogenic and natural sources (Smedley and Kinniburgh, 2001).

Redox potential (Eh) and pH are identified by Hounslow (1980) and Smedley and Kinniburg (2002) as the two main driving factors in determining arsenic speciation and solubility in subsurface aquifers. Soluble arsenic is most commonly observed in one of two oxidation states, arsenate [As(V)] and arsenite [As(III)] (Smedley and Kinniburgh, 2002). In oxidizing environments, arsenate species (H_3AsO_4, $H_2AsO_4^-$, $HAsO_4^{2-}$, and AsO_4^{3-}) are dominate (Figure 2-A, B) (Saunders et al., 2008). The arsenate tends to be mobile under oxidizing conditions and its speciation is highly pH dependent, however, arsenate can heavily sorb onto iron and manganese oxy-hydroxide (FeOOH and MnOOH) coatings if present in the environment in question (Saunders et al., 1997).

Under reducing conditions the more toxic arsenite is the dominant form of dissolved arsenic. Arsenite can be mobile or immobile in reducing conditions depending on several factors. Under moderately reducing conditions arsenite in the form of the dominant aqueous species, $As(OH)_3$, is mobile. If the aquifer becomes increasingly reducing to the point of sulfate reduction in low iron, sulfur-rich conditions, solid arsenic sulfide complexes such as orpiment (As_2S_3) and realgar (AsS) (immobilized) or thioarsenite aqueous complexes such $As(SH)_4^-$ (mobile) would likely form (Figure 2-A) (Saunders et al., 2008). If an aquifer contains sulfur rich conditions and dissolved iron concentrations are high, the arsenite will become immobile as it will incorporate itself into Fe-sulfides such as arsenian-pyrite (e.g., $FeS_{1.99}As_{.01}$). The arsenic will also adsorb onto the surface of the mineral and precipitate out of the system, effectively being sequestered from the system (Figure 2-B) (Huerta Diaz and Morse, 1992; Saunders et al., 1997; Saunders et al., 2008; Smedley and Kinniburgh, 2002). Several laboratory studies have shown that arsenic may be removed from solution via adsorption or co-precipitation on Fe-sulfide solids such as

mackinawite, troillite, pyrite, and arsenian-pyrite (Bostic and Fendorf, 2003; Han et al., 2013; Le Pape et al., 2017; Wolthers et al., 2005).

The geochemistry of arsenic speciation in natural waters, its tendency to be effectively absorbed onto, and integrated into the crystalline structure of iron sulfide minerals has given rise to the idea of utilizing this as a technique to remediate arsenic-contaminated groundwater (Zouboulis et al., 1993; Jingtai and Fyfe, 2000). Further research on this process has shown several advantages in using iron sulfide minerals to sequester arsenic as a viable bioremediation technique in the field. Firstly, the formation of arsenian-pyrite has been shown to be thermodynamically more favorable than the formation of solid arsenic sulfide minerals like orpiment or realgar in natural waters (Saunders et al., 2008). Arsenian-pyrite has also been shown to be relatively stable under changing redox conditions, indicating this process is a stable sink of arsenic (Deflaun et al., 2009; Onstott et al., 2011). Lastly, research by Saunders et al. (2005b; 2008) has shown that through an added amendment, native populations of sulfate reducing bacteria can be stimulated and cause shifts in pH and Eh conditions that favor the formation of arsenian-pyrite in shallow arsenic contaminated aquifers. This allows aquifers to be engineered into conditions which favor biogenic pyrite formation and arsenic sequestration.

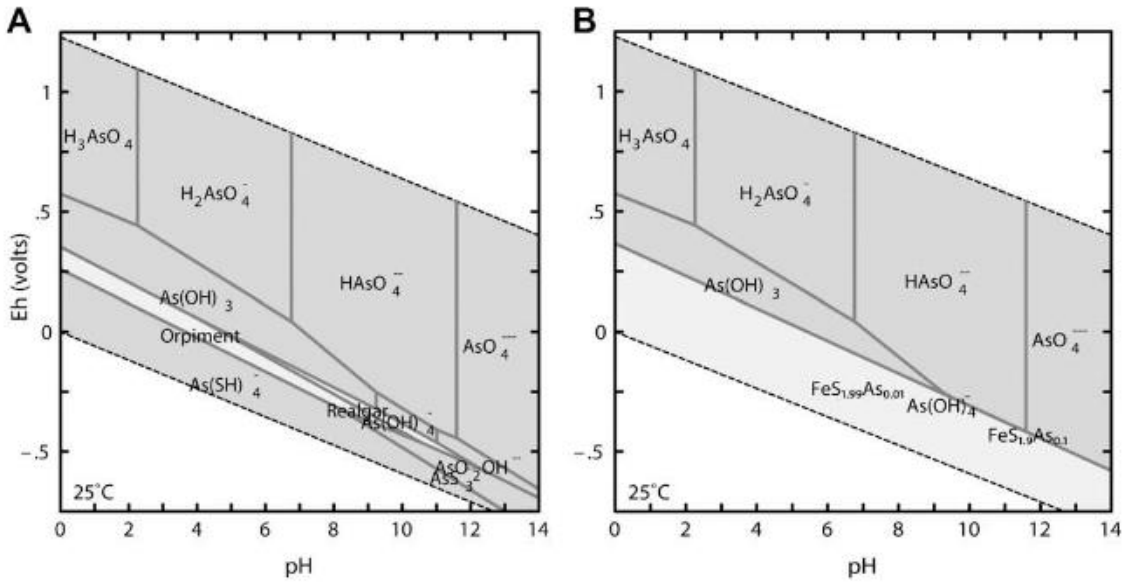

Figure 2. (A) Eh-pH diagram for arsenic speciation in an As-S-O_2-H_2O system at 25 degrees Celsius and 1 bar of pressure plotted in Geochemist Workbench. (B) Eh-pH diagram for arsenic speciation in an As-Fe-S-O_2-H_2O system at 25 degrees Celsius and 1 bar of pressure plotted in Geochemist Workbench (Saunders et al., 2008).

The bioremediation technology employed in this study utilizes these geochemical properties of arsenic, while optimizing the growth of sulfate reducing bacteria and the formation of biogenic pyrite (pyrite formed through the induced changes caused by micro bacteria) in an attempt to reduce arsenic concentrations in the groundwater below the EPA's standard. This study furthers the research of Starnes (2015), Saffari (2015), and Levitt (2016) at an industrial site in Florida where the groundwater is heavily contaminated with herbicide-based arsenic. The main objective of this study is to gain a better understanding of the pyrite-grain formation that takes places during the bioremediation process that has been initiated at this Florida field site. This was done by analyzing the pyrite grains that formed naturally by SRB before stimulation and comparing them to both the pyrite-grains that formed as a result of the stimulation and subsequent sulfate reduction as well as the pyrite-grains that remain in the sediment post sulfate reduction. Since there is scant published research on the long-term stability of newly formed iron sulfide phases under changing redox and hydrologic conditions, this gave a comprehensive analysis of the effectiveness of bioremediation process over the yearlong monitoring. Differences in the sulfur isotope ratios of sulfate in groundwater, as well as pyrite's crystal structure and chemical compositions, especially the amount of arsenic incorporated per unit mass of biogenic grain, were analyzed using multiple techniques. This study also focuses on imaging the nano-particle sized pyrite grains to determine characteristic texture and distribution throughout the sediments sampled during this study.

Modeling was also conducted to determine time series relationships of biochemical reactions along flow pathways as well as the ultimate efficiency of the arsenic removal rate in groundwater by pyrite biomineralization. Additional modeling was conducted using data collected throughout this study to further affirm the notion that arsenian-pyrite is more

thermodynamically favorable than other arsenic sulfide phases in this low-temperature setting. Lastly, a geochemical reaction path model was used to determine the limiting reagents for this reaction as a way to both refine and optimize the recipe of the amendments injected to increase pyrite production and to ultimately lower the dissolved arsenic concentrations in the groundwater. The results of this study provide biogeochemical data on how effectively arsenic is being sequestered as a direct result of the bioremediation technology that can be employed and refined at field scale.

Background

A yearlong arsenic bioremediation study was conducted from February 2016 to February 2017 at a Florida industrial site. The site is a 0.3 acre industrial substation, located in northwest Florida (Figure 3). This site was heavily polluted with arsenic trioxide stemming from the usage of herbicides. From 1989 to 1993, contamination assessments verified that contamination level in groundwater was well above EPA limit of 0.05 mg/L and had spread offsite (Mintz and Miller, 1993). Initial remediation began in 1992 with the excavation of 770 cubic yards of contaminated soil. This directly led to a 40% decrease in the arsenic concentration and a significant decrease in the size of the contamination plume. This excavation was followed by the installation of a pump-and-treat system to further the remediation effort. However, this expensive form of ex-situ remediation was ended in 1999 after failing to bring arsenic levels in the groundwater below both EPA and Florida Department of Environmental Protection (FDEP) standards.

The study site is located on the Gulf of Mexico on the Apalachicola Embayment in the panhandle of Florida (Figure 3) (Schmidt & Clark, 1980). Using data obtained from the United States Geological Survey (USGS) (Schweitzer, 2017), a Geographic Information System (GIS)

map was constructed showing the lithology of Bay County. The main lithology is unconsolidated, undifferentiated sediments composed of clay, silt, sand, and gravel size particles of Pleistocene to Holocene age. The study area is located within this lithologic unit.

The subsurface hydrogeology at the site can be characterized into three main hydrological units (Schmidt and Clark, 1980). The contamination that occurred at the site has affected the top aquifer (Surficial Aquifer). The Surficial Aquifer is mainly composed of quartz sand and gravel. The water table at the study site is very close to the surface (4-7 ft.). The Surficial Aquifer at the site is underlain by a clay rich confining unit named the Jackson Bluff Formation, which acts as a barrier, restricting flow from the Surficial Aquifer downward to the other hydrostratigraphic units (Schmidt and Clark, 1980). Consequently, this restricts the advective transport of arsenic downward to the other hydrologic facies and helps confine the contamination to the Surficial Aquifer (Schmidt and Clark, 1980).

In early 2015, Auburn University geoscience graduate student Peter Starnes surveyed the Surficial Aquifer by collecting and analyzing groundwater samples in available monitoring wells (Starnes 2015) in order to get baseline information before remediation. The average arsenic levels observed at this site were around 150 ppb, with levels reaching as high as 577 ppb (Starnes, 2015). Relatively low oxidation-reduction potential (ORP), low dissolved oxygen levels (DO), and elevated levels of ferrous iron (Fe^{2+}), all indicate that the redox conditions of at the site are moderately reducing. The arsenic speciation was also analyzed and arsenite was found to be the dominant arsenic species (Starnes, 2015).

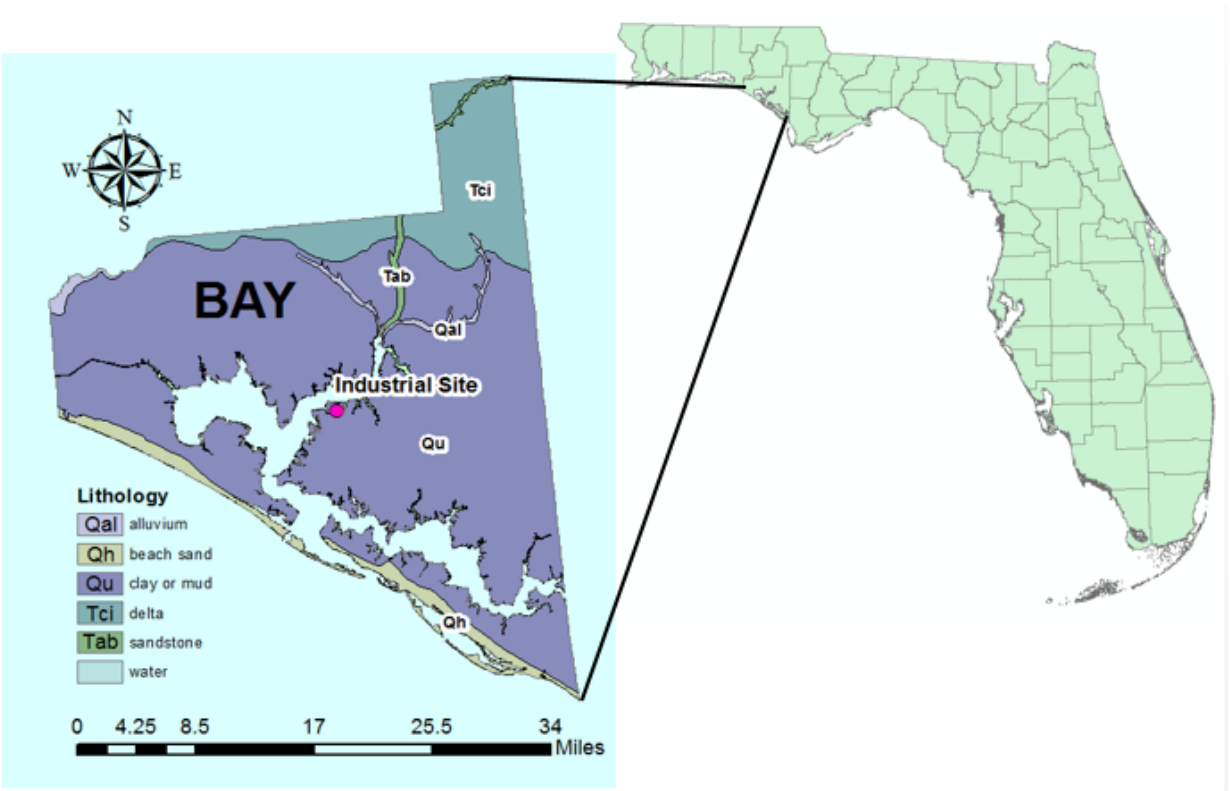

Figure 3. Geologic map of Bay County, Florida, including the location of the study area.

Starnes (2015) also determined the optimal amendments required to shift the environment from a moderately reducing to a sulfate reducing environment. His geochemical models showed that an addition of hydro ferrous sulfate ($FeSO_4 \cdot 7H_2O$) and a labile organic carbon source would effectively achieve this shift in conditions. However, the model did not quantify the amounts of amendments required to sequester dissolved arsenic at the site below the maximum concentration limit. Additionally, his hydrological models determined the groundwater flow of the aquifer to be about 20 m/yr to the west-northwest. Thus the migration of the contamination plume extends to the northwest carrying the arsenic off site.

In February 2016, Auburn University geoscience graduate students Shahrzad Ghandehari and Eric Levitt began the process of drilling four wells (two monitoring and two injection wells) to facilitate the remediation process. The locations of the monitoring and injection wells are shown in Figure 4. The monitoring wells (M-1, M-2) were drilled downgradient to the northwest of the injection wells (I-1, I-2) in accordance with the hydraulic gradient of the aquifer. The two injections wells were stimulated with a combination of water, molasses (labile organic carbon source), hydro ferrous sulfate ($FeSO_4 \cdot 7H_2O$), and fertilizer to stimulate the indigenous SRB (Ghandehari, 2016). Injection well 1 (I-1) was stimulated with a 2000 gallon solution mainly consisting of water with added constituents including of 5 Kg of $FeSO_4$, 27.2 kg of molasses, 0.9 kg of agricultural grade fertilizer in 1,000 gallons of water. The solution injected into I-1 was considered the weak solution due to the relatively small amount of added hydro ferrous sulfate. Injection well 2 (I-2) was stimulated with a 1000 gallon solution mainly consisting of water with added constituents including of 2.5 kg of $FeSO_4$, 27.2 kg of molasses, 0.9 of fertilizer. This solution was considered the strong solution due to the high proportion of $FeSO_4$ amendments to

water. The two injection wells were stimulated with solutions of different strengths to determine if this would have an effect on the SRB and make one solution more effective than the other (Ghandehari, 2016).

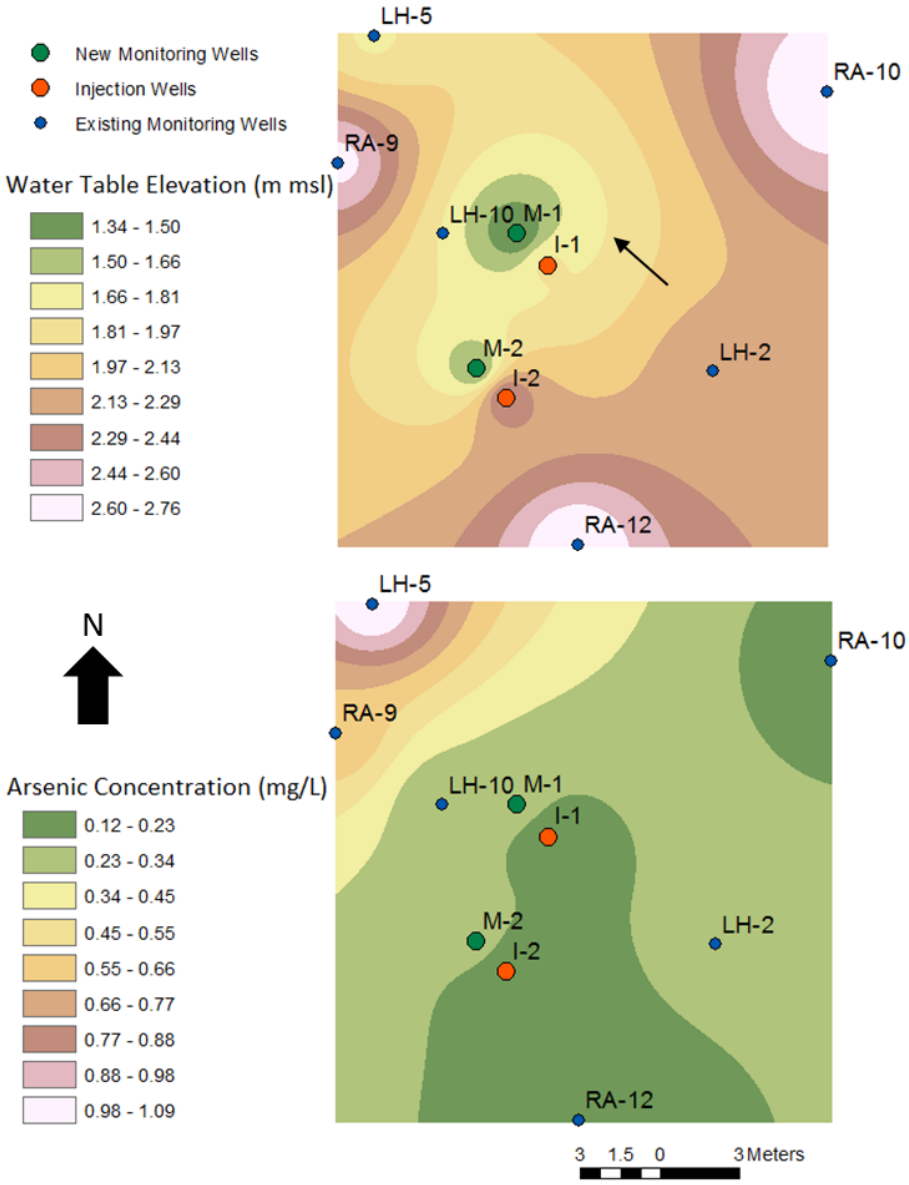

Figure 4. Maps displays the location and distribution of injection wells (I-1, I-2), newly installed monitoring wells (M-1, M-2), and existing monitoring wells at the field site as well as the direction (arrow) of groundwater flow. The upper map displays pre-injection water table elevations and the lower map displays the arsenic concentration distributed in the groundwater (Adapted from Ghandehari, 2016).

Methodology

Field Sampling & Sediment Processing

Sediments were sampled 11 times from the ten wells highlighted in Figure 4 during the yearlong study, weekly for the first month and then bimonthly for the rest of the year. The solid sediments samples that accumulated through gravity settling were collected from the bottom of the wells using a peristatic pump and silicone tubing and placed in one-liter plastic bottles. These bottles were immediately placed in coolers containing dry ice with limited headspace (to preserved redox conditions). These bottles were stored in a freezer until the sediments were processed.

The processing of these sediments begins by first thawing and dewatering the bottles taken from the field. The dewatering process was conducted in two different ways. The first method of dewatering was done by transferring as much solid particulates from the one-liter bottles to much smaller 50 mL centrifuge vials. The vials, labeled with the specific well the sediments were collected from, were then centrifuged for approximately ten minutes at 3000 rotations per minute (rpm). Once centrifuged the excess liquid was drained, the wet sediments were transferred to ceramic crucibles to be subsequently dried on a hotplate, and transferred to small, labeled plastic bags. This would often take several days for the sediments to completely dry using this method. The other method of dewatering consisted of pouring the thawed sediment slurry through Whatman Grade 2, 8 micrometer pore sized filter paper. The filter paper was then dried on a hotplate and the sediment transferred to small, labeled plastic bags. This filter dry method took around a day for the sediments to completely dry. After drying the sediments were ready for imaging and geochemical analysis. Though sediments were collected from all 10

wells, the sediments collected from the injection wells (I-1, I-2) and wells closest in proximity to the injection wells (M-1, M-2), were the focus of this study.

Changes in Arsenic Concentrations and Water Chemistry

Major ion concentrations of the groundwater were determined through analysis on an Agilent 7900 quadrupole inductively coupled plasma mass spectrometry (ICP-MS) at Auburn University. Anion concentrations were measured using a Dionex 2000 ion chromatograph (IC). The arsenic concentration in the three most proximal monitoring wells to the injection wells (M-1. M-2, and LH-10) were examined and plotted verse time. This was done to determine the timeline in which arsenic could be effectively sequestered below the site's regulatory clean up standard of 0.05 mg/L with the volume of injectant solution used to stimulate sulfate reduction. The concentrations of iron, sulfate, hydrogen sulfide, and arsenic from monitoring well M-2 were also plotted verse time so important changes in the chemistry of the ground water could be observed. These data were essential in determining a timeline for shifting redox conditions and optimal arsenic sequestration.

Geochemical Analysis

X-ray diffraction (XRD), X-ray fluorescence (XRF), and electron microprobe (EMP) analyses were the principal studies used to geochemically characterize the biomineralized iron sulfide sediments. The use of these techniques to study the time-series structure and compositional changes between the pyrite grains allowed for a determination of a comprehensive picture of this process.

XRD is widely used to identify unknown crystalline materials and fine-grained material (Bish and Post, 1989). Therefore, this analysis was helpful in identifying the predominant

minerals present in the recovered sediments, especially pyrite and other iron sulfides. The processed sediments were powdered and analyzed using standard operating procedure for a Bruker D2 Phaser X-ray Diffractometer. When the processed sediment volume was not enough to fill a standard Bruker powdered sample holder the sediment would be instead mounted on a zero background glass sample holder. The resultant XRD spectra was analyzed using the DIFFRAC.EVA software. This software, using Bragg's Law, converts the dominant peaks detected on the spectra to d-spacings, which can be searched and matched to the unique d-spacings of known minerals thus identifying the mineral composition of the sediments. This analysis was conducted at the XRD-XRF laboratory in the Department of Geosciences at Auburn University.

Information including the bulk chemical makeup as well as trace metal detection can be gathered using X-ray fluorescence (Fitton, 1997). The XRF analysis conducted in this study was used to characterize the bulk elemental composition in the sediments including the presence of arsenic in the sediments in a semi-quantitative manner. The XRF analysis of the powdered, processed sediments was conducted on a portable Bruker Elemental IV-ED XRF in the Auburn University Geosciences Department.

Electron microprobe analyzer (EMP) was also used for a high-precision chemical analysis of the minerals found in the processed sediments. Unlike the XRF analysis, EMP's can analyze spots on mineral grains as small as 1-2 microns in diameter in a quantitative manner (Reed, 2005). Thus this was used to look at compositional changes across a single pyrite grain and more importantly to quantify the amount of arsenic per unit mass of pyrite grain. Sediments were mounted on glass slides with epoxy and polished using a combination of sandpaper and micron sized diamond grit. After polishing the samples were ready for analysis on the EMP.

Using standards for iron, sulfur, and arsenic, the pyrites were located in the polished samples and analyzed using wavelength dispersive spectrometers (WDS) automated with the probe for Advanced Microbeam EMP software. The EMP analysis was conducted in the Geosciences Department using the JEOL-8600 at Auburn University.

The sulfur isotope signatures of pyrite formed can be used to fingerprint the progress of bacterial sulfate reduction in treated groundwater. SRB have a well-known kinetic isotope effect on dissolved sulfate (SO_4) (Thode et al. 1951; Lee and Saunders 2000) by preferentially using lighter ^{32}S in metabolism. The produced H_2S and associated pyrite tend to be enriched in ^{32}S. The sulfur isotope signatures of dissolved sulfate in treated groundwater were measured at the Colorado Plateau Stable Isotope Laboratory at Northern Arizona University using standard combustion techniques and analyzed by a Thermo Electron gas isotope-ratio mass spectrometer. Dissolved SO_4 is precipitated out of water samples as $BaSO_4$ by the addition of $BaCl_2$. Sulfur isotope signatures of both pyrite solids and dissolved sulfate were used collectively to fingerprint the progress of bacterial sulfate reduction.

Imaging Analysis

A scanning electron microscope (SEM) analysis allows the users to image, measure, and examine variations in morphology of extremely small objects (Reed, 2005). An SEM analysis was conducted using a Zeiss EVO 50VP scanning electron microscope at the Auburn University Instrumentation Facility to compare the size and texture of the pyrite grains formed at different stages of bioremediation. Sediments for this analysis were prepared by mounting on a conductive holder and then sputter-coated with gold.

Geochemical Reaction Modeling

Geochemist's Workbench (GWB) (Bethke, 2008) was used to model the speciation of arsenic under various Eh-pH conditions, saturation index of arsenian-pyrite at field site, mineralogic reactions and groundwater chemistry changes in response to field biostimulation by added amendments. Thermodynamic data for thioarsenite species, amorphous As and Fe sulfide phases, and arsenian-pyrite were compiled (Table 1) into a revised GWB database for the speciation calculations.

Table 1. Equilibrium constants (at 25°C) for the formation of thioarsenites, arsenic sulfides, iron sulfides, and arsenian-pyrite used in geochemical modeling.

Reactions	log K_{25}	References
Thioarsenite species		
$As(OH)_4^- + HS^- + 2H^+ \Leftrightarrow As(OH)_2(SH) + 2H_2O$	17.92	(*Wilkins et al., 2003)*
$As(OH)_4^- + HS^- + H^+ \Leftrightarrow As(OH)_2S^- + 2H_2O$	12.77	(*Wilkins et al., 2003)*
$As(OH)_4^- + 2HS^- + H^+ \Leftrightarrow As(OH)S_2^{2-} + 3H_2O$	17.83	(*Wilkins et al., 2003)*
$As(OH)_4^- + 3HS^- + 2H^+ \Leftrightarrow AsS_3H^{2-} + 4H_2O$	29.61	(*Wilkins et al., 2003)*
$As(OH)_4^- + 4HS^- + 4H^+ \Leftrightarrow As(SH)_4^- + 4H_2O$	45.77	(*Wilkins et al., 2003)*
$As(OH)_4^- + 3HS^- + H^+ \Leftrightarrow AsS_3^{3-} + 4H_2O$	21.72	(*Wilkins et al., 2003)*
Arsenic sulfides and iron sulfides		
$2As(OH)_4^- + 3HS^- + 5H^+ \Leftrightarrow As_2S_3$ (Orpiment) $+ 8H_2O$	65.60	*(Webster, 1990)*
$2As(OH)_4^- + 3HS^- + 5H^+ \Leftrightarrow As_2S_{3\,(am)} + 8H_2O$	63.27	*(Webster, 1990)*
$As(OH)_4^- + HS^- + 2H^+ \Leftrightarrow AsS$ (Realgar) $+ 3.5H_2O + .25\ O_{2(aq)}$	14.68	*(Bethke, 1996)*
$Fe^{2+} + 2HS^- + .5\ O_{2(aq)} \Leftrightarrow FeS_2$ (Pyrite) $+ H_2O$	59.29	(*Wilkins, 1996; Schoonen, 1991)*
$.875\ Fe^{2+} + HS^- + .0625\ O_{2(aq)} \Leftrightarrow FeS_{.875}$(Pyrrhotite) $+ .75\ H^+ + .125\ H_2O$	9.88	(*Wilkins, 1996*; *Schoonen, 1991)*
$Fe^{2+} + HS^- \Leftrightarrow$ FeS (Mackinawite) $+ H^+$	3.10	*(Webster, 1990)*
$Fe^{2+} + As(OH)_4^- + HS^- \Leftrightarrow$ AsFeS (Arsenopyrite) $+ 2.5H_2O + .75\ O_{2(aq)}$	-47.84	*(Bethke, 1996)*
Arsenian pyrite		
$FeS_{1.99}As_{0.01} + 1.02\ H_2O + 3.5\ O_2(aq) \Leftrightarrow Fe^{2+} + 1.995\ SO_4^{2-} + 0.01\ As(OH)_4^- + 2\ H^+$	199.78	(*Saunders et al., 2008*)

Results and Discussion

Changes in Arsenic Concentrations and Water Chemistry

Arsenic concentrations increased to several mg/L in affected downgradient wells (M-1, M-2) two weeks after the injection, but began to decrease quickly from the third week (Figure 5). After a few weeks, arsenic levels in three affected wells decreased significantly from 0.25-0.34 mg/L to below 0.05 mg/L (Figure 5). After about one month, the site regulatory clean-up goal for arsenic of 0.05 mg/L had been reached in all three affected wells, and remained below that for at least 6 months in M-1 and M-2. Arsenic concentration in the deeper LH-10 well dropped below 0.05 mg/L over the entire year of monitoring after injection. The total Fe concentrations in M-1 and M-2 increased to more than 100 mg/L one week after injection (Figure 6) compared to the pre-injection levels (< 1 mg/L). Dissolved sulfate concentrations in these wells also increased to hundreds of mg/L after injection (Figure 6). The concurrent increase in arsenic and ferrous iron concentrations right after injection might be resulting from bacterial iron reduction. Iron-reducing bacteria compete with SRB for organic carbon and they can cause arsenic release (Chapelle and Lovley, 1992). Amendments of nutrients in wells might also cause initial arsenic release because phosphate and nitrate can compete with arsenic for sorbing sites on aquifer minerals (Neumann et al., 2010; Aziz et al., 2016). Fe, SO_4, and As levels in affected wells show concurrent decreases in the third week, followed by a decrease in H_2S in the 4th week, consistent with SRB mediated precipitation of pyrite and removal of arsenic from groundwater (Figure 6). Thus H_2S produced by SRB apparently reacted with dissolved Fe (or perhaps Fe in solid phases) to make pyrite capable of removing arsenic by sorption and co-precipitation.

As stated above the arsenic concentrations remained below the regulation level of 0.05 mg/L in these affected wells for at least 6 months (from March to September). After the six

month principal sequestration stage, there is an increase of the arsenic concentration in the groundwater. Changes in the water table elevations were compared to arsenic concentration to see if a correlation could be made (Figure 7). The drop in the water table between early October and December appears to correlate with the initial increases of the arsenic concentration. This decline in the water table perhaps caused a short-lived oxidation of sulfide solids and remobilization of arsenic. However, the observed arsenic increases in M-1 and M-2 were not accompanied by concurrent increases in Fe or SO_4 (Figure 6), suggesting limited oxidation of biogenic pyrite. Couture et al. (2013), in a previous lab experiment, showed that only around 2% of previously sequestered arsenic in pyrite re-dissolve into solution under aerobic conditions, indicating the stability of this sink. As discussed above, groundwater migrates at the rate of about 20 m/y in a general direction from southeast to west-northwest. Thus the arrival of untreated groundwater from up-gradient would also cause an increase in arsenic concentrations during the latter part of the experiment. Overall, the arsenic concentrations after September were still below the pre-injection level in affected wells. The arsenic levels in the LH-10 well did not show a significant shift in response to hydrologic or meteorological changes. This could be due to its relatively deeper water table that is less sensitive to fluctuations in water table elevation or to its position further hydrologically downgradient where the untreated groundwater has not arrived yet.

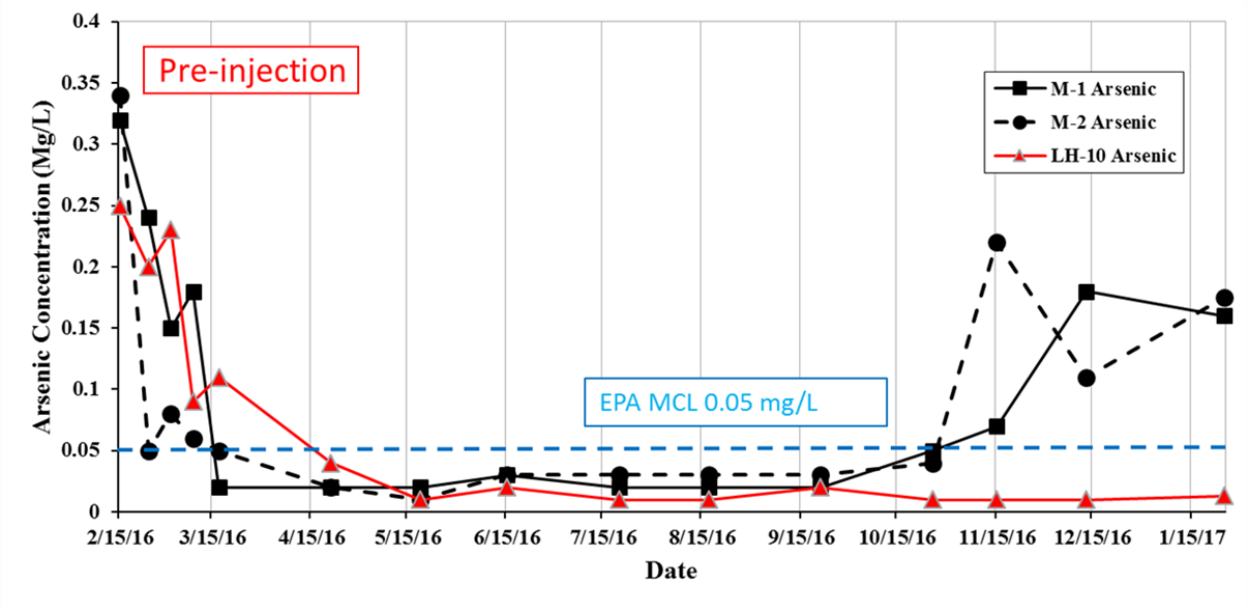

Figure 5. Plot of arsenic concentration in the groundwater in the three most proximal monitoring wells to the injection site (M-1, M-2, and LH-10) compared to the sites regulatory clean up goal for the yearlong study period.

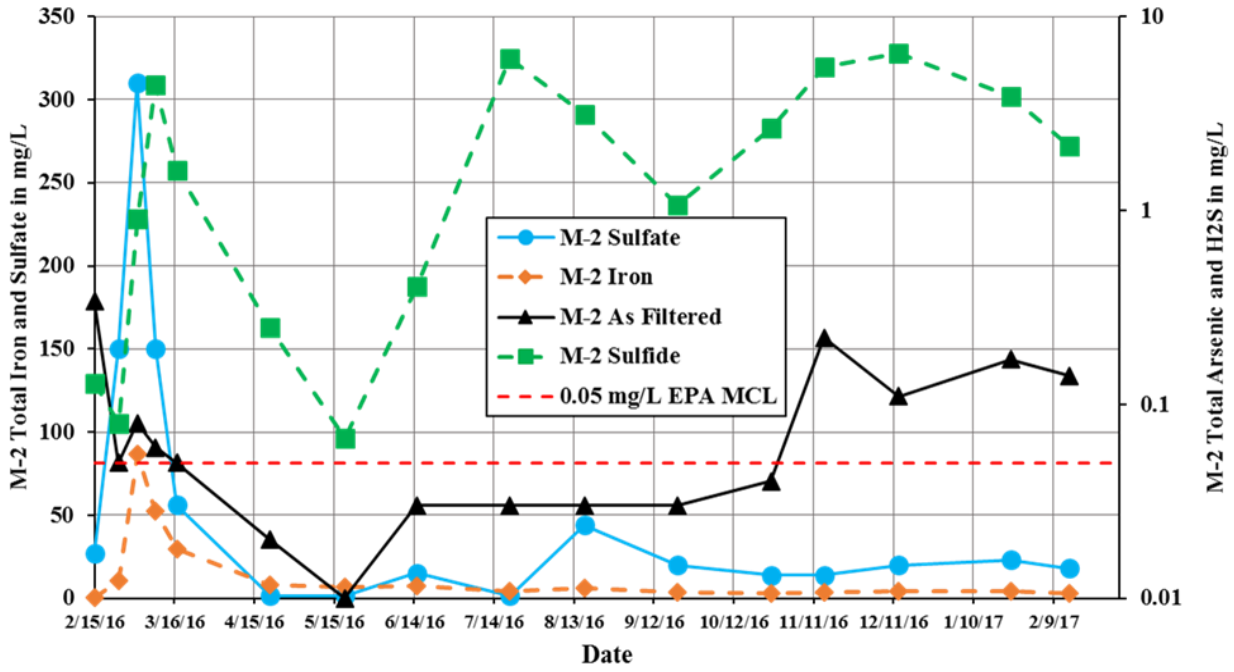

Figure 6. Plots showing dissolved iron, sulfate, sulfide, and arsenic concentrations in monitoring well M-2 throughout the yearlong study period.

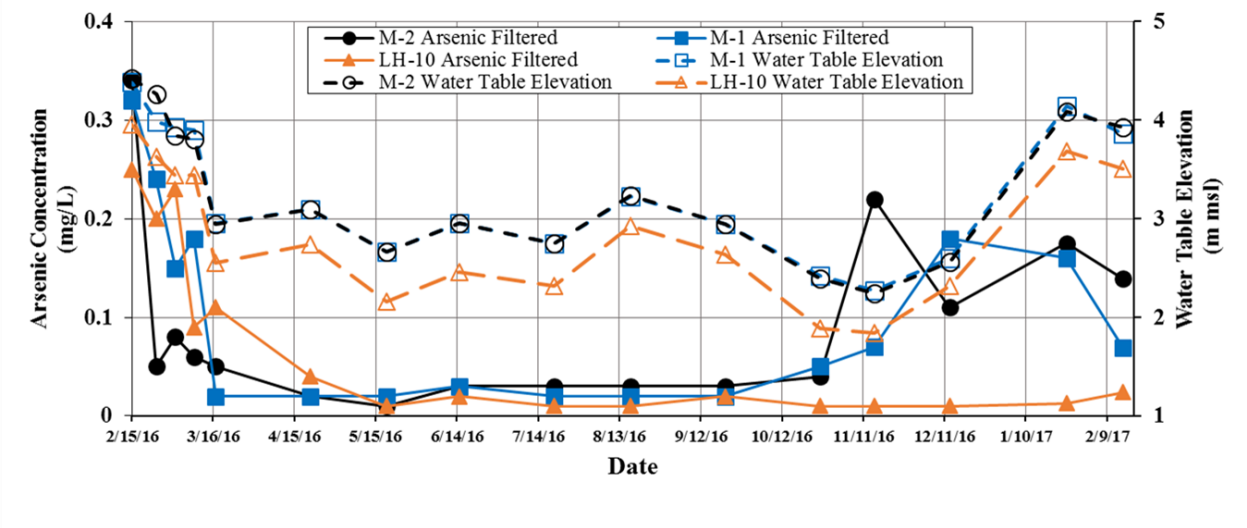

Figure 7. Plot of arsenic concentration in the groundwater in the three most proximal monitoring wells to the injection site (M-1, M-2, and LH-10) compared to fluctuations in water table elevation.

Geochemical Analysis

The results of the XRD analysis (Figure 8 and 9) display the spectra of neo-formed solids recovered from M-1 and M-2 respectively, throughout the one year monitoring period. When analyzed in DIFFRAC.EVA software, the sediments were found to contain mainly three minerals, arsenian-pyrite (COD 9013070), kaolinite (COD 9009230), and Quartz (COD 5000035). The arsenian-pyrite that DIFFRAC.EVA software closely matched to the iron sulfide phase found in the sediment samples was reported in Reider et al. (2007) with a chemical formula of $As_{0.026}FeS_{1.974}$. This arsenian-pyrite came from a lignite deposited in the Czech Republic. The peak positions of arsenian-pyrite (COD 9013070) and pyrite (COD 9013069) in Figures 6 and closely match arsenian-pyrite spectrum at 2θ = 28.5°, 33.0°, 37.0°, 40.7°, 47.3°, and 56.2°. The spectrum peak for the arsenian-pyrite formed in the early stages of the bioremediation process (M-1 - March 2nd, 2016; M-2 – February 24th, 2016) increases in its intensity in the following months of analysis (April and June) and maintain a prominent peak for the duration of the yearlong samplings period, indicating the stability of the arsenian-pyrite in the sediments. No other iron sulfide or arsenic sulfide phases were identified in this XRD analysis.

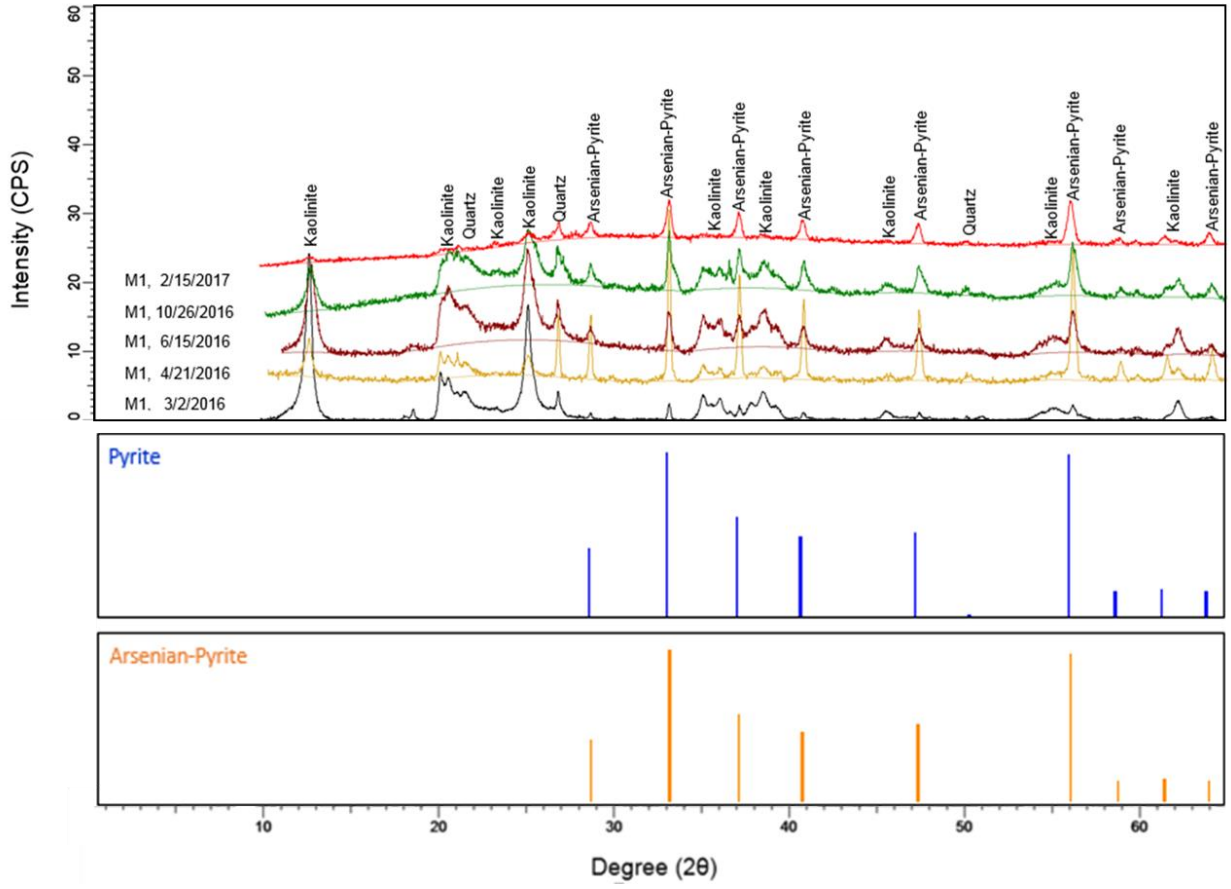

Figure 8. XRD spectra for M-1 sediments sampled throughout the yearlong bioremediation field study compared to known peak intensities and locations for both pyrite and arsenian-pyrite

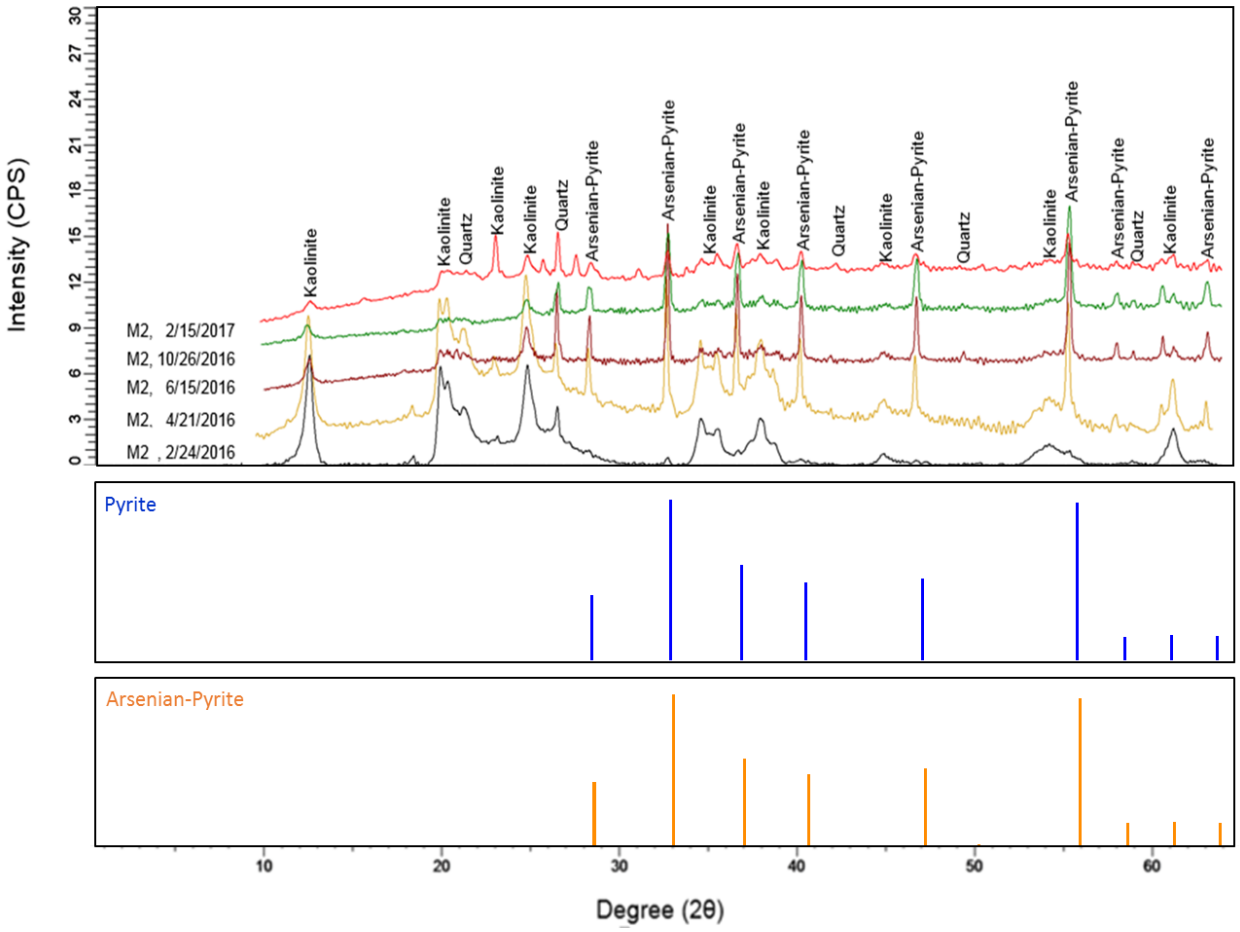

Figure 9. XRD spectra for M-2 sediments sampled throughout the yearlong bioremediation field study compared to known peak intensities and locations for both pyrite and arsenian-pyrite.

The XRF analysis yielded strong evidence for the formation of arsenian-pyrite as the spectra produced had consistently strong peaks for iron, sulfur, and arsenic as highlighted in Figures 10 and 11. These figures represent the XRF analysis for sediments sampled from M-1 and M-2 on March 17th, 2016 or one month post injection. These results are consistent with the XRD analysis. The EMP analysis also confirms the formation of arsenian-pyrite. Two polished thin sections were prepared using sediments from I-2 during two different stages of the bioremediation process, April (early stage) and October (late stage). Forty-three arsenian-pyrite grains were analyzed from the April thin section, while thirty-seven were analyzed from the October thin section. The arsenic content in the arsenian-pyrites were fairly consistent for both sampling periods, ranging from 0.05 to 0.40 weight percentage arsenic (Figure 12), which could indicate the effective sequestration potential of arsenic in this form of biogenic pyrite.

Lastly, the results of the sulfur isotope analysis reveal a significant sulfur isotopic fractionation resulting from bacterial sulfate reduction (Figure 13), There is a direct correlation between the amount of SO_4 and H_2S in the groundwater and the enrichment of the $\delta^{34}S$ isotope in dissolved sulfate of groundwater. During the active bacterial sulfate reduction process (high levels of SO_4 and H_2S) the sulfate remaining in the groundwater was enriched with $\delta^{34}S$ by 2-4‰. This indicates the bacteria are preferentially selecting the lighter $\delta^{32}S$ when reducing sulfate into hydrogen sulfide (Thode et al., 1951). In wells where no bacterial sulfate reduction occurred water was only slightly enriched in $\delta^{34}S$ by 0.44-0.66‰, thus indicating background sulfur isotope ratios.

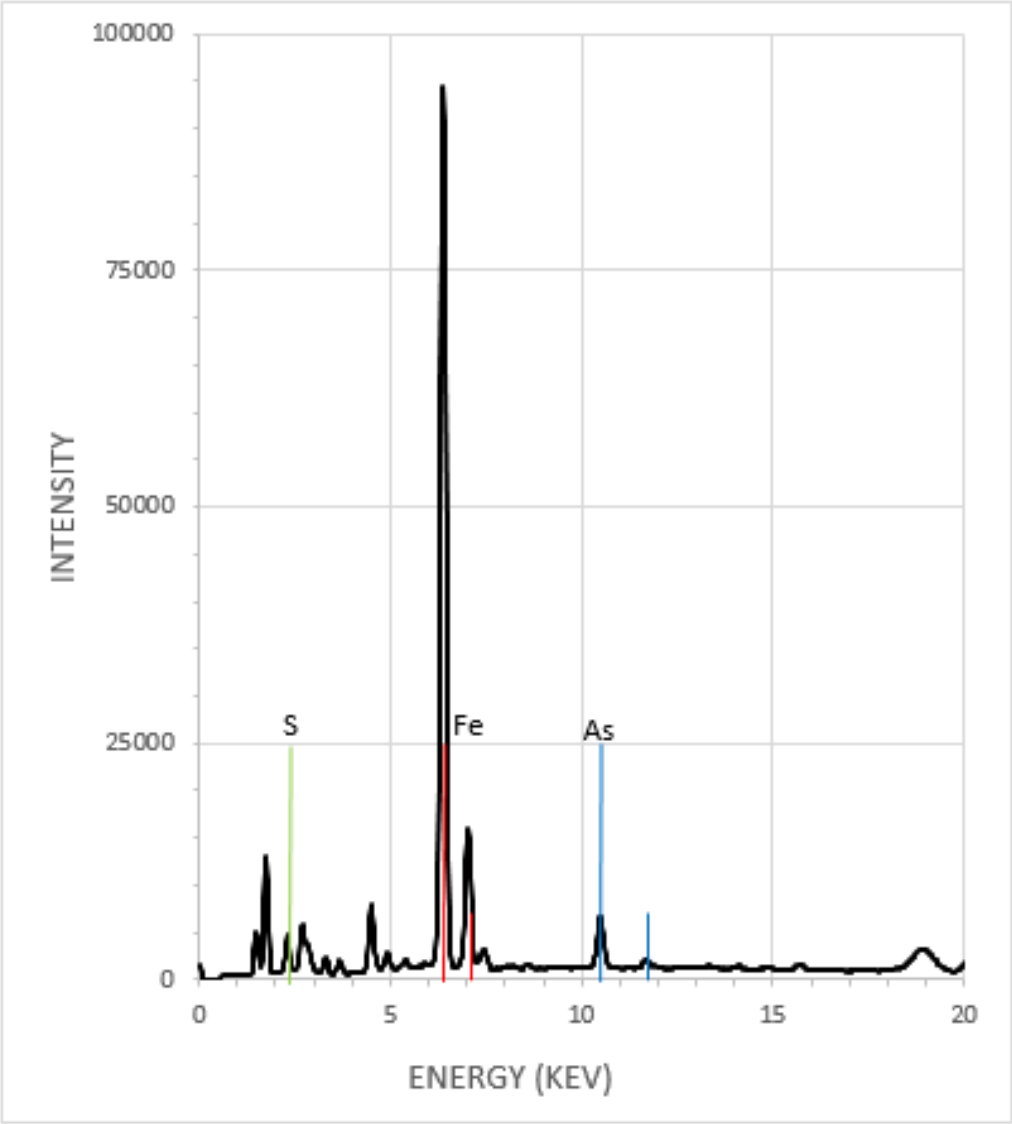

Figure 10. XRF spectra for sediments collected from M-1 one month after biostimulation, the peak location of sulfur, iron, and arsenic are highlighted.

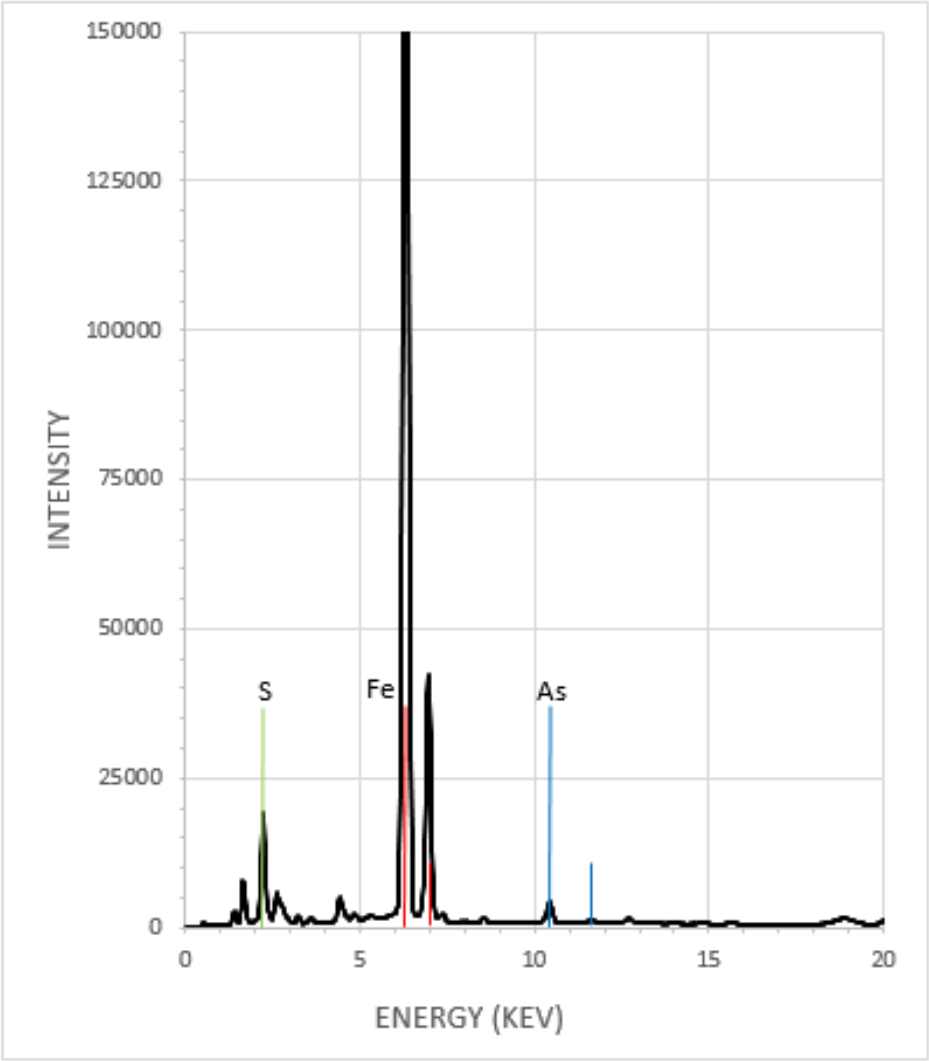

Figure 11. XRF spectra for sediments collected from M-2 one month after biostimulation, the peak location of sulfur, iron, and arsenic are highlighted.

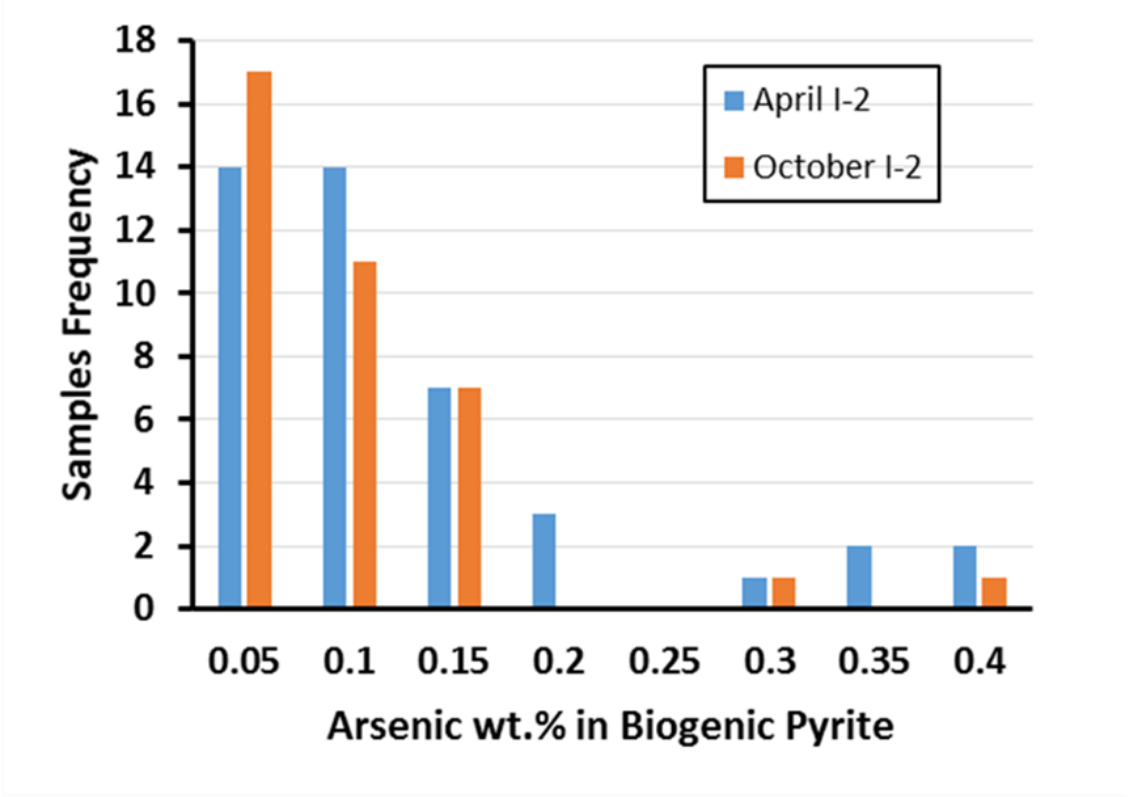

Figure 12. Histogram of arsenic weight percentages measured by the EMP for sediments sampled from I-2 in April and October.

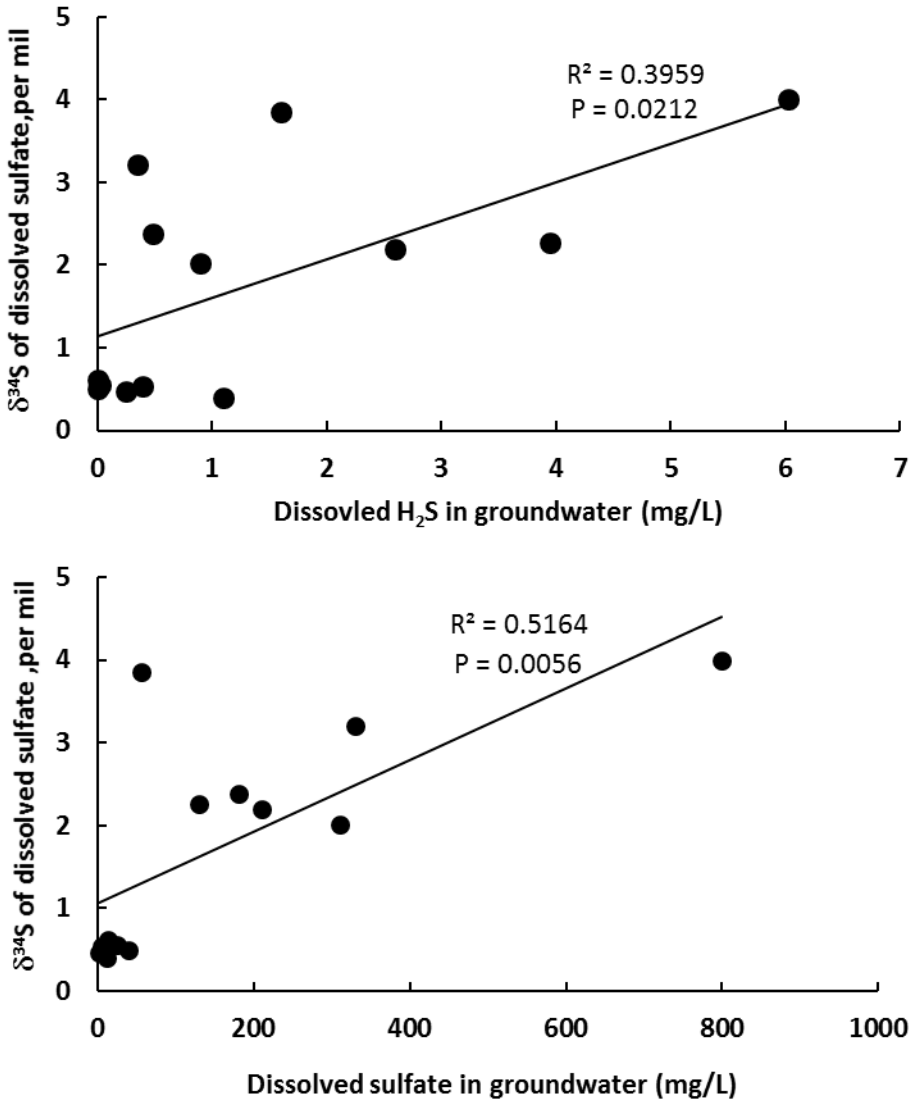

Figure 13. Two plots indicating the sulfur isotope composition of the dissolved sulfate in the sampled groundwater (‰, relative to Canyon Diablo meteorite, CDT) relative to the concentration of dissolved H_2S and SO_4 during this study.

Imaging Analysis

The SEM imaging analysis lent more confirmation to the presence of arsenian-pyrite in the recovered sediments. This analysis imaged and compared sediments sampled from M-2 during the March 9th 2016 sampling period, two weeks post biostimulation (Figures 14A, C, 15-18) and October 2016 (Figures 14B, D; 19-21) sampling periods. The results showed that the pyrite grains were present in two principal morphologies, euhedral crystals (Figures 14D, 18) and spherical aggregates of nanocrystalline-sized pyrite grains or framboids (Figures 14 A,C-17, 19). This well-formed framboidal aggregates ranged in size from 10-50 micrometer (μm) in diameter, while the well-formed euhedral crystals were smaller and ranged in size from 1-10 μm. This framboidal pyrite morphology has been observed to develop in laboratory experiments when ferrous iron and hydrogen sulfide react and pyrite rapidly precipitates (<12 hours) (Gartman and Luther, 2013). Thus the presence of this morphology lends suggests that the arsenian-pyrite observed in the sediments sampled from the field site formed through rapid precipitation.

In addition to the well-formed framboids, Figures 14B, 20, 21 display the loosely assembled, weathered remains of framboids. This was only observed in the sediments analyzed from October and indicates that the well-formed framboids observed in the sediments imaged early on in this study will disassemble into these clusters of nano-sized crystalline pyrite during the later stages of the bioremediation process. Besides this morphological difference between pyrite framboids, there were other differences observed in the pyrites imaged early in the bioremediation process as compared later stages. Greater numbers of crystalline pyrite were observed in the October sediments. Also the thin biofilm-like materials that naturally attached on the surface of these framboids increased in volume to the extent that intact framboids were

difficult to recognized in the October sediments as compared to the easily recognizable framboids observed in the March sediments.

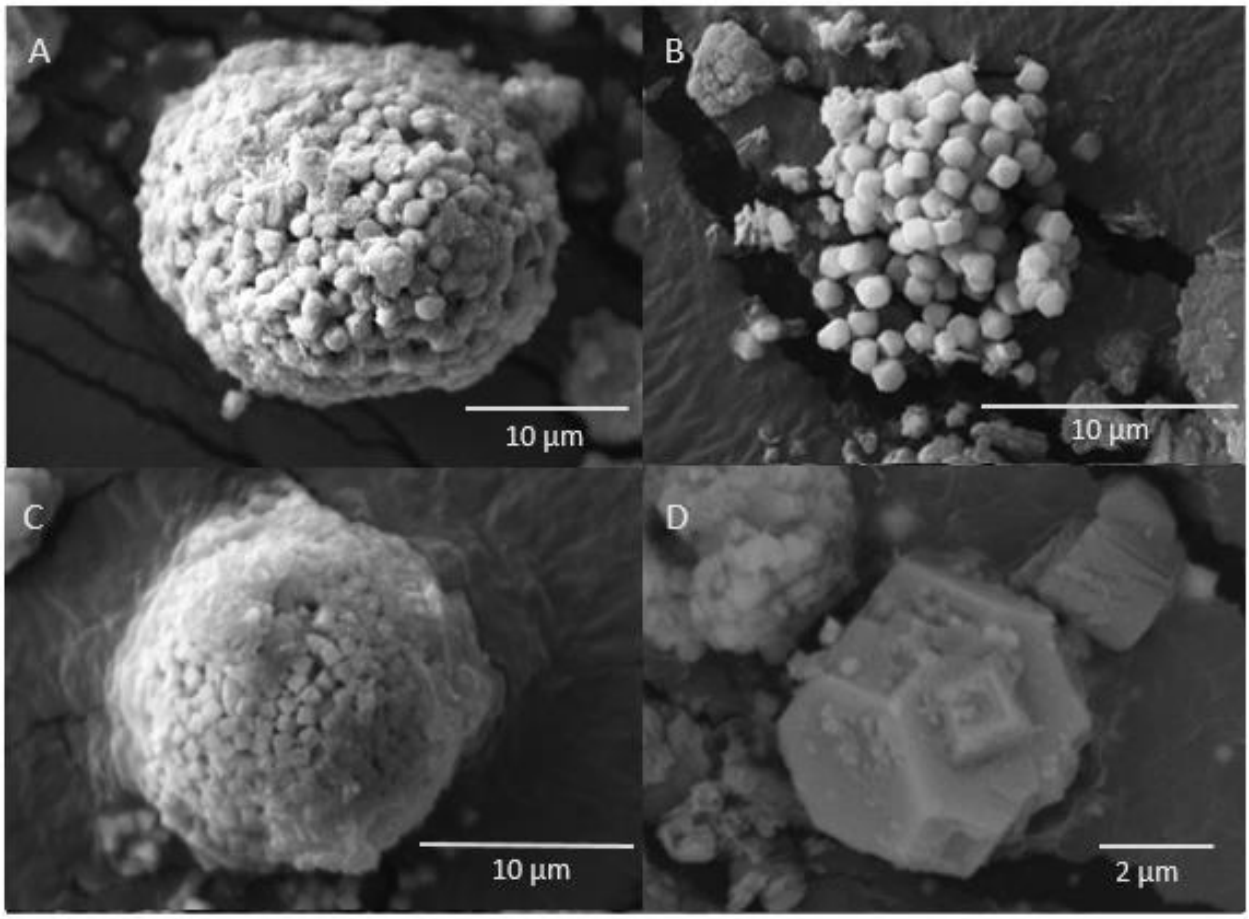

Figure 14. SEM image comparison of the pyrite morphology that formed at two stages (A, C March 9th 2016; B, D October 2016) of bioremediation.

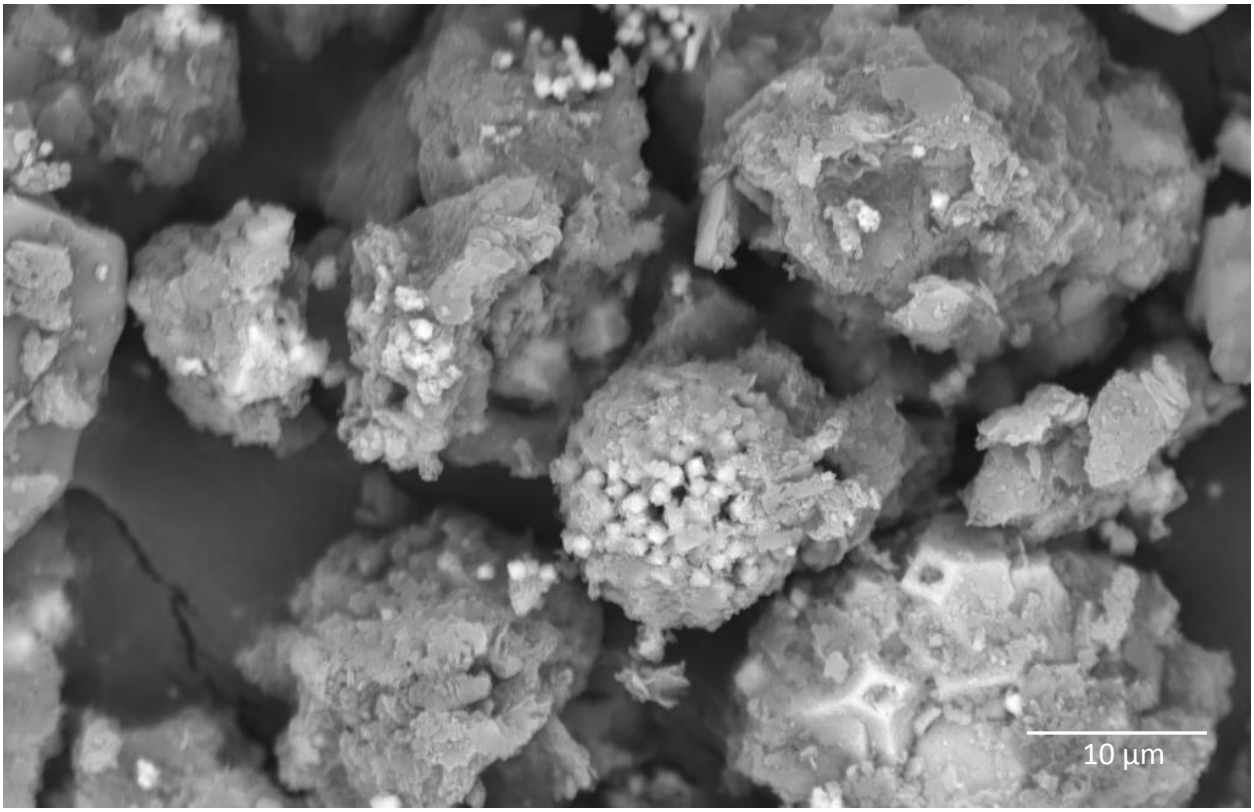

Figure 15. SEM backscatter image of a 10 µm diameter pyrite framboid at five thousand times magnification from sediments sampled from M-2 two weeks post biostimulation.

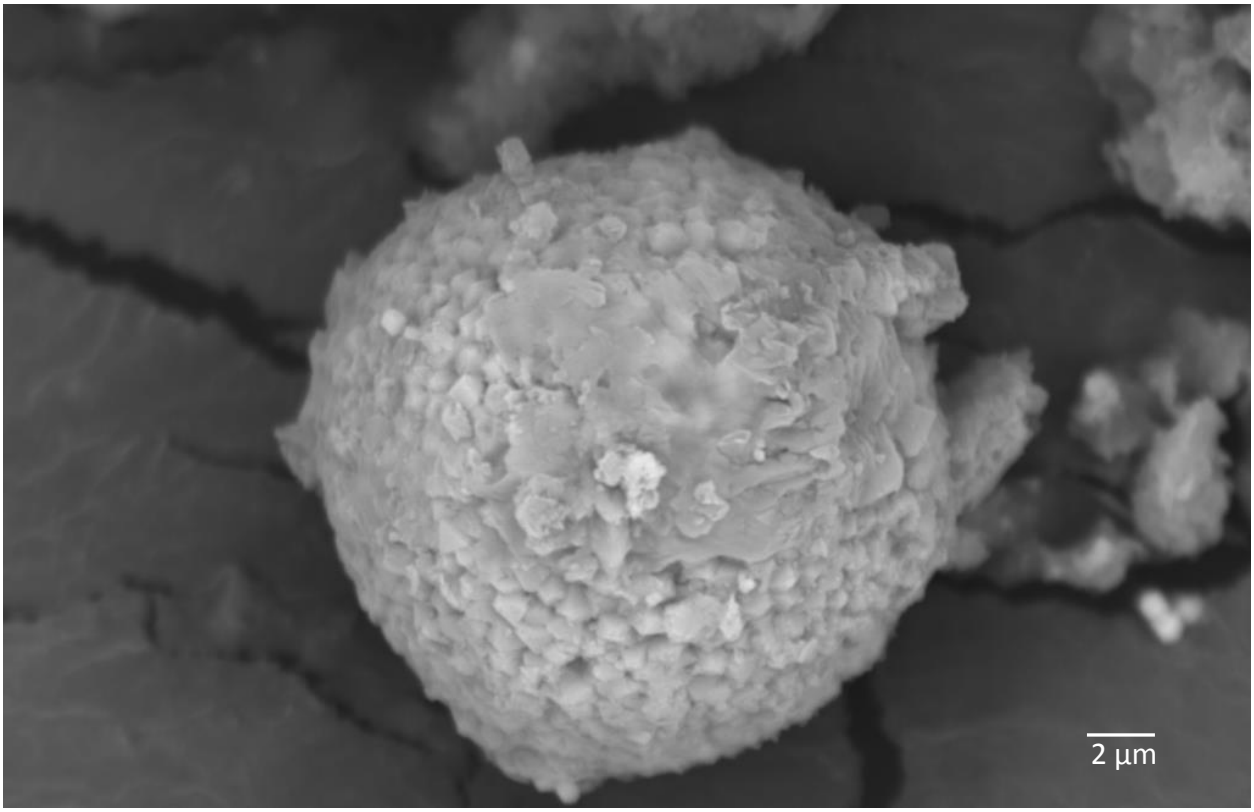

Figure 16. SEM backscatter image of a 17 µm diameter pyrite framboid at ten thousand times magnification from sediments sampled from M-2 two weeks post biostimulation.

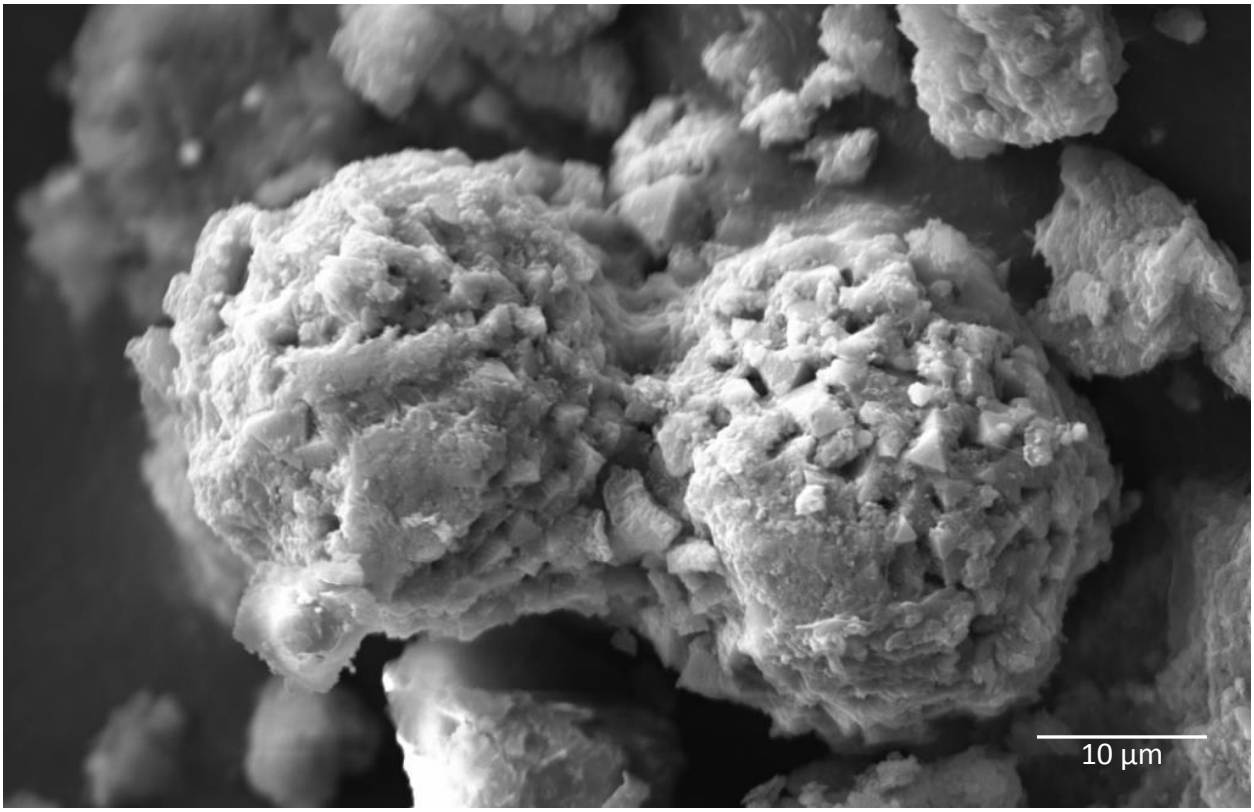

Figure 17. SEM image of 10 µm diameter twinned pyrite framboids at five thousand times magnification from sediments sampled from M-2 two weeks post biostimulation.

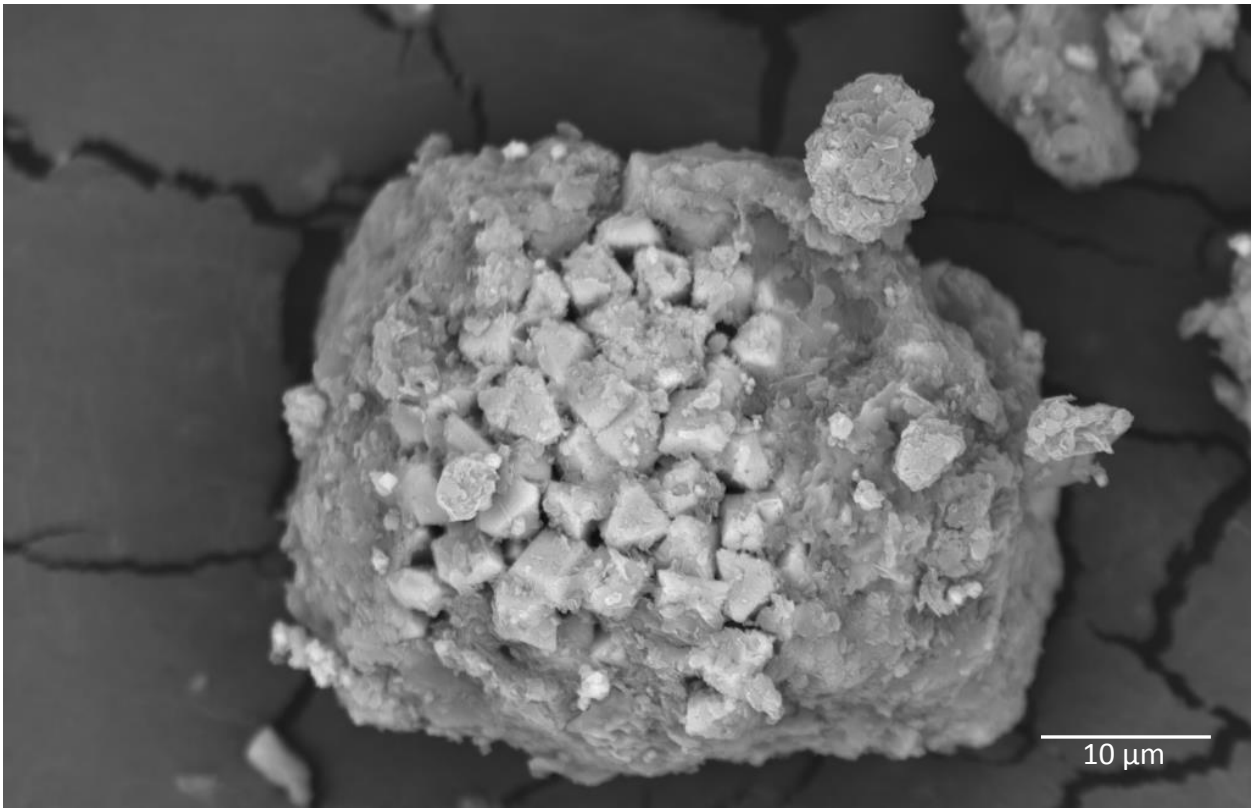

Figure 18. SEM backscatter image of 2 µm euhedral pyrite crystals at ten thousand times magnification from sediments sampled from M-2 two weeks post biostimulation.

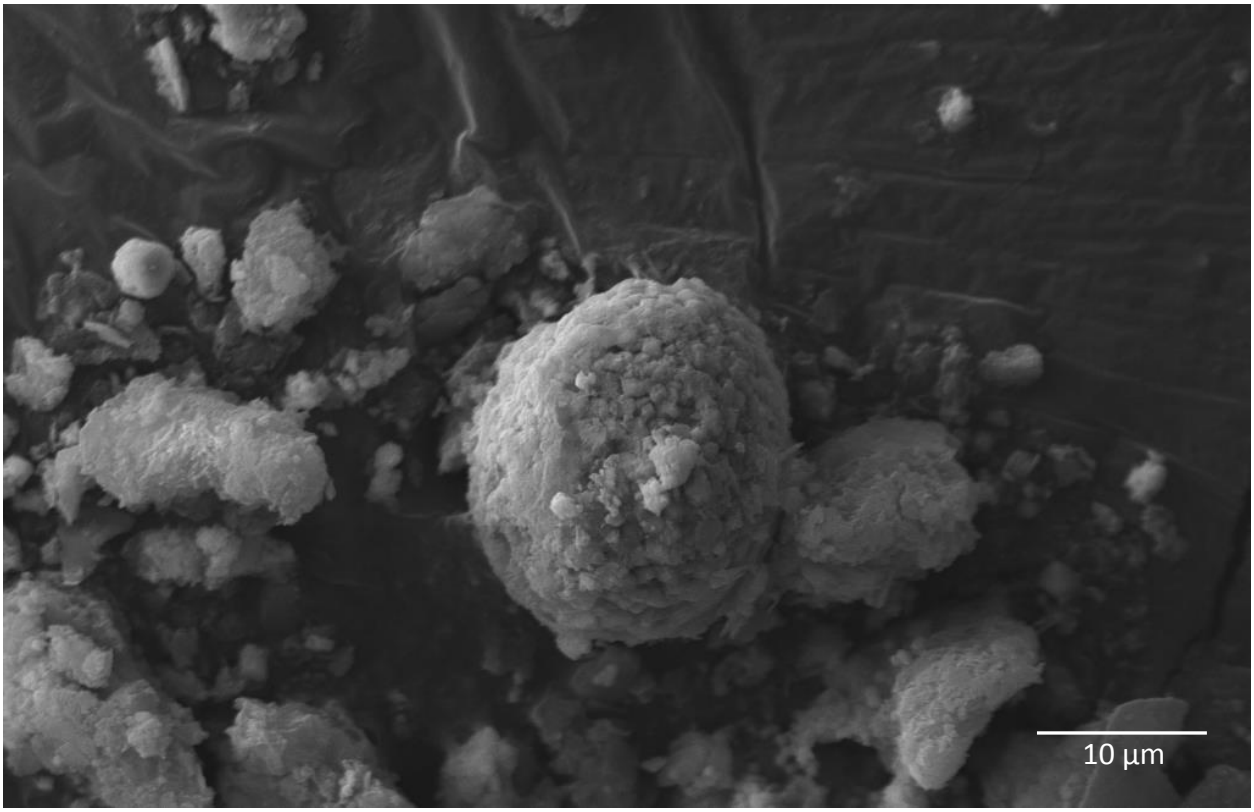

Figure 19. SEM image of a 15 µm pyrite framboid at five thousand times magnification from sediments sampled from M-2 during October.

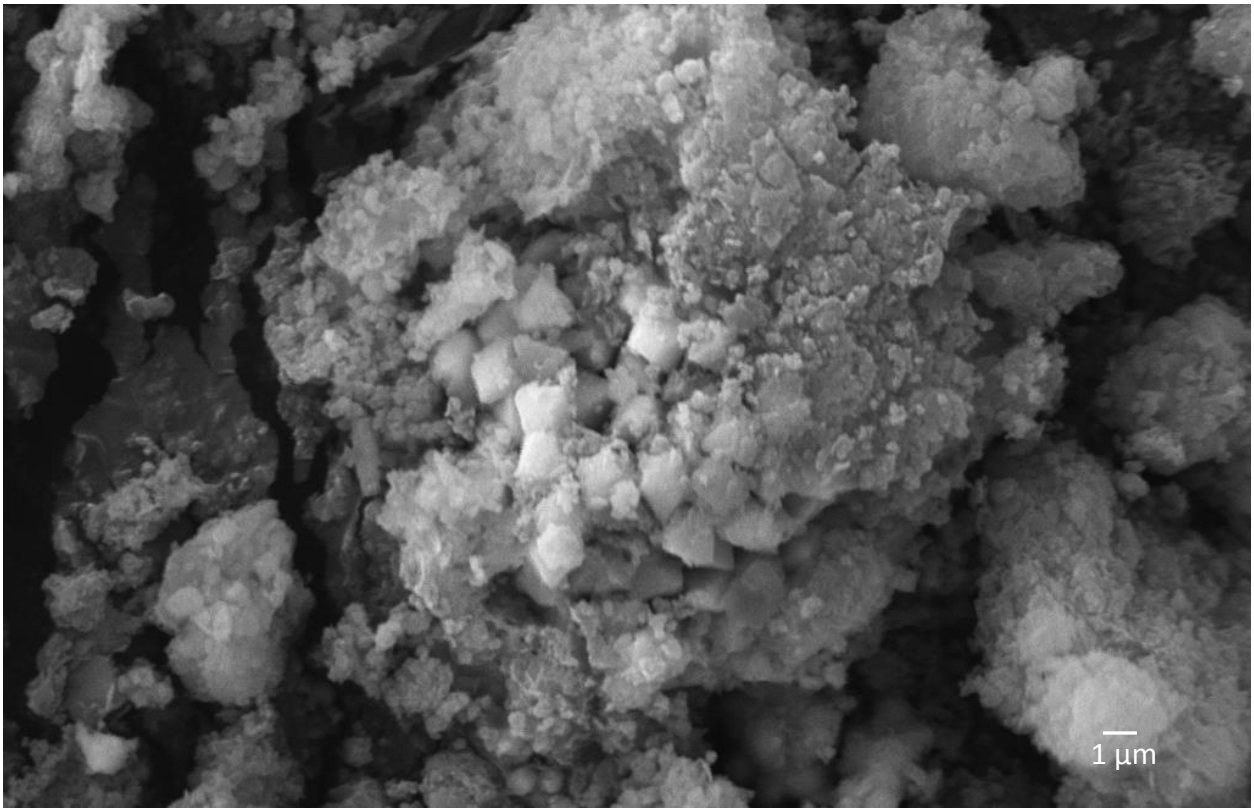

Figure 20. SEM image of a cluster of 1 µm euhedral pyrite crystals at ten thousand times magnification from sediments sampled from M-2 during October.

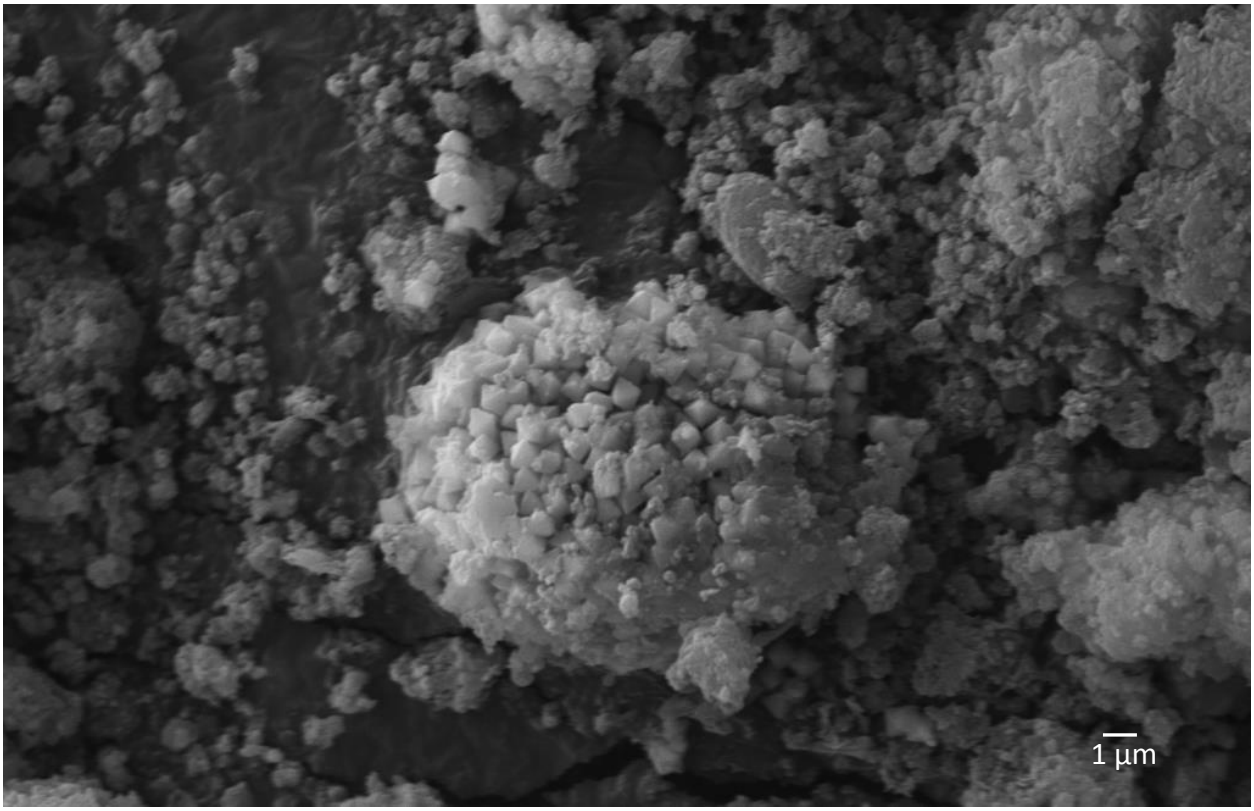

Figure 21. SEM image of a 15 µm loosely assembled pyrite framboid at ten thousand times magnification from sediments sampled from M-2 during October.

Spatial and Temporal Geochemical Analysis

Spatial and temporal changes in the groundwater geochemistry was assessed and modeled using several different calculations. These calculations tracked the injectant plumes movement downgradient (Figure 22), evaluated the fraction of arsenic removed by conservative mixing versus biomineralization (Figure 23), and quantified the saturation index for arsenian-pyrite along a flow transect (Figure 24). Figure 22 displays breakthrough curves showing the arrival of the injectant plume at different wells along a flow transect (I-1, M-1, LH-10, RA-9, and the up-gradient LH-2). Using a conservative chloride tracer, which was known to have a concentration of 200 mg/l in the fertilizer of the initial injectant solution, the arrival of the center of mass of injectant plume could be observed as a spike in the concentration of chloride in the groundwater at each well. The main processes responsible for the movement of the conservative tracer downgradient was advection and hydrodynamic dispersion.

The arrival of the center of mass of chloride tracer was also estimated using Darcy's Law. Using a hydraulic conductivity of 400 m/yr, a hydraulic gradient of 0.010-0.015, a porosity of 30 percent, a flow velocity of 20 m/yr (parameters taken from Starnes, 2015), and assuming advective transport, the peak concentration of the chloride trace arrived at M-1 around 30 days, at LH-10 around 75 days, and at RA-9 around 175 days. When compared to the actual arrival time of the conservative tracer from the chloride concentration in the groundwater the plume arrived earlier than estimated for well M-1. This is most likely caused by a greater hydraulic gradient at the point of injection. Farther down the flow transect (LH-10 and RA-9) the chloride tracer arrives later than what was estimated by Darcy's Law. This was most likely caused by descreased hydraulic gradient or increased dilution and diffusion of the injectant plume as it flowed down gradient.

The mixing ratio of the injectant solution with the groundwater was important when determining what fraction of arsenic removed (as compared to pre-injection concentrations) was actually caused by the sequestration of arsenic into arsenian-pyrite verse diluted by the injectants. Figure 22 shows the aresenic removal fraction in the groundwater and the mixing ratio of the injectants as measured in both M-1 and M-2 wells throughout the yearlong study. The mixing ratio (w) was calculated using the following equation:

$$w = \frac{C_{mixed} - C_{pre-injection}}{C_{injectate} - C_{mixed}}$$

The variables $C_{pre\text{-}injection}$, $C_{injectate}$, and $C_{mixed,}$ represent the chloride concentration in the pre-injected groundwater, the injectant solution, and the mix of these two fluids throughout the duration of this study. This figure shows that after peak sulfate reduction is established in April, more than 90% of the dissolved arsenic is removed from the groundwater in both wells. In this same time the mixing ratio of the chloride tracer remained below well below 20% for M-1 and below 10% for M-2. This indicates that the removal of arsenic was only minimally affected by dilution (<20%), with a majority of the arsenic being removed from the sequestration and precipitation of the arsenian-pyrite (>80%).

The saturation index (SI = log IAP/log K) of arsenian-pyrite was calculated to determine when and where the geochemical conditions favored the precipitation of arsenian-pyrite along a flow transect (I-1, M-1, LH-10, RA-9, and the up-gradient LH-2). The log K value of arsenian-pyrite and its chemical formula used in calculations is shown in Table 1. The results showed (Figure 23) that the SI of the pre-injection groundwater in these wells along this flow transect with respect to arsenian-pyrite was negative, indicating undersaturation and conditions unconducive for arsenian-pyrite precipitation. One week after injection, arsenian-pyrite became

saturated (positive SI) in wells LH-2, I-1, and M-1 indicating the precipitation of this mineral phase. In contrast, it took the wells located further downgradient, LH-10 and RA-9, several months to become saturated (2 and 6 months respectively). The shift back to undersaturated conditions in I-1 during the last couple months, most likely was caused by inflows of contaminated water from up-gradient. The geochemical conditions in these wells maintained saturation during the main sequestration stage (until September and October) indicating the stability of these pyrites that served as a sink for dissolved arsenic.

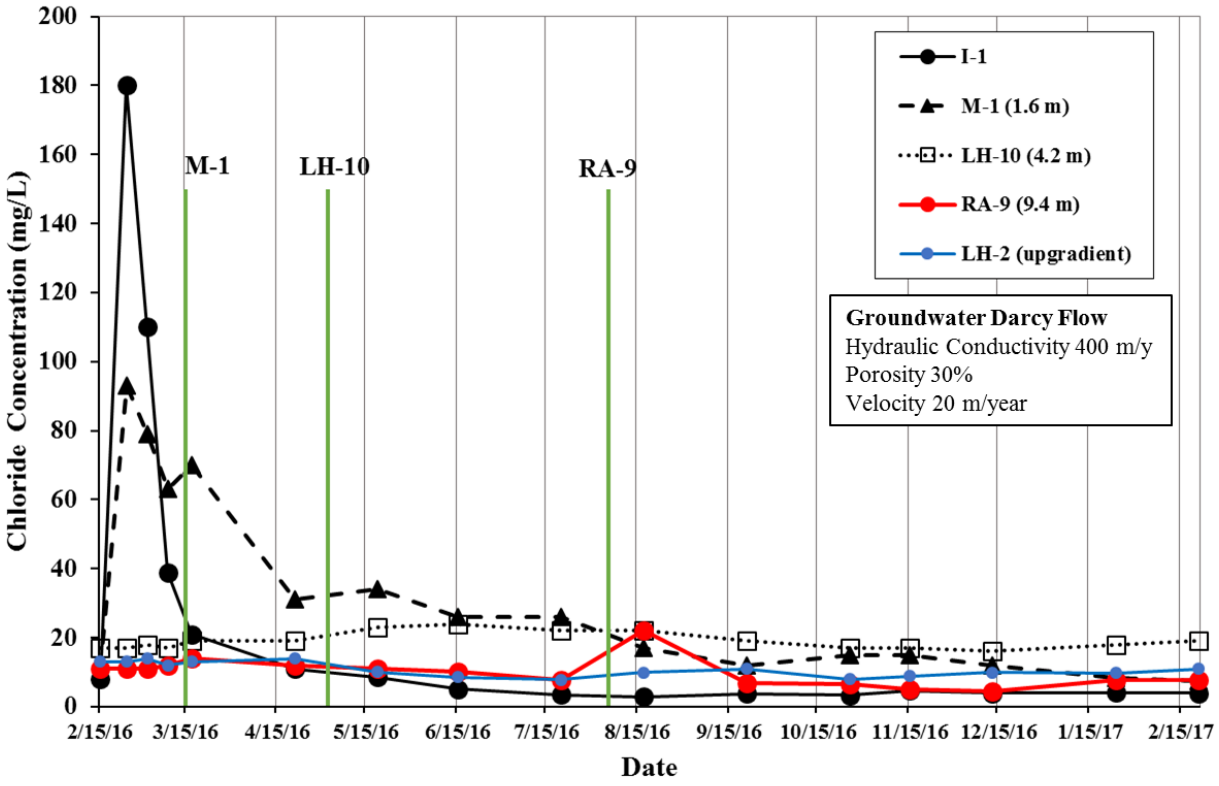

Figure 22. Breakthrough curve diagram showing the arrival of the conservative chloride tracer as well as the estimated arrival time for this transect of wells.

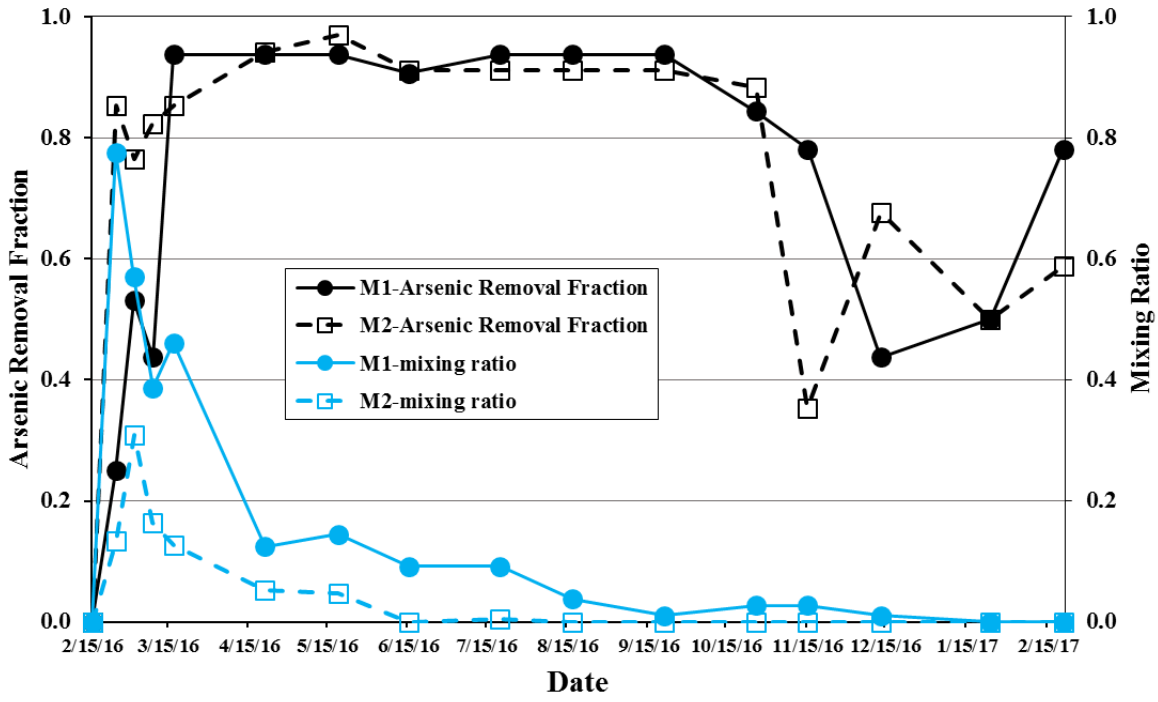

Figure 23. Plot evaluating the dilution effect by comparing the arsenic removal fraction with the mixing ratio in the groundwater of wells M-1 and M-2.

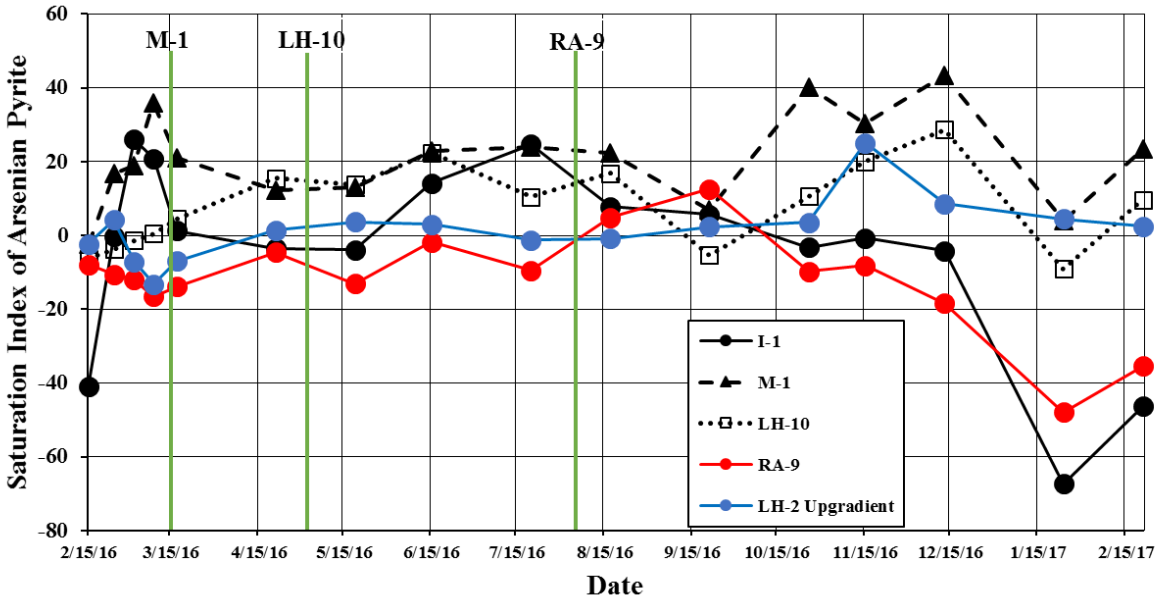

Figure 24. Plot showing the changes in the saturation index (indicating the precipitation potential of the arsenian-pyrite mineral phase) along this transect of wells throughout the field study.

Geochemical Reaction Modeling

Geochemical modeling was conducted using GWB (Bethke, 2008) to assess arsenic speciation, predict mineralogical reactions along reaction paths, and estimate the arsenic sequestration potential of arsenian-pyrite using site specific conditions. The first model (Figure 25), was created to assess the capacity of other possible arsenic sulfide minerals, specifically amorphous orpiment, are able to sequester arsenic in a low temperature setting with minimal soluble iron concentrations. Using the Act2 program within GWB, an activity-activity diagram was constructed with the activity of the arsenic species $As(OH)^-$ on the y axis and the activity of H_2S on the x axis. This stability diagram was plotted at varying pH values (4, 6, and 8) to show how the solubility of amorphous orpiment (as activity of $As(OH)_4^-$) changes with pH and activity of H_2S. This model shows that amorphous orpiment becomes more soluble as arsenic forms thioarsenite aqueous complexes AsS_2^- or $As(SH)_4^-$ at high activity of H_2S. Orpiment becomes less stable and arsenic becomes more mobile when the solution contains minimal H_2S. This model also shows that amorphous orpiment becomes increasingly insoluble with decreasing pH. However as indicated by the model the formation of amorphous orpiment under various geochemical conditions is not sufficient to lower arsenic activities at or below the EPA's maximum contaminant level (MCL) of 10 ug/L, or with activity around 10^{-7} (horizontal line). Therefore these modeling results demonstrate that the amorphous orpiment does not have the sequestration capabilities to serve as a viable sink of arsenic at concentrations low enough to comply with the EPA's drinking water standard.

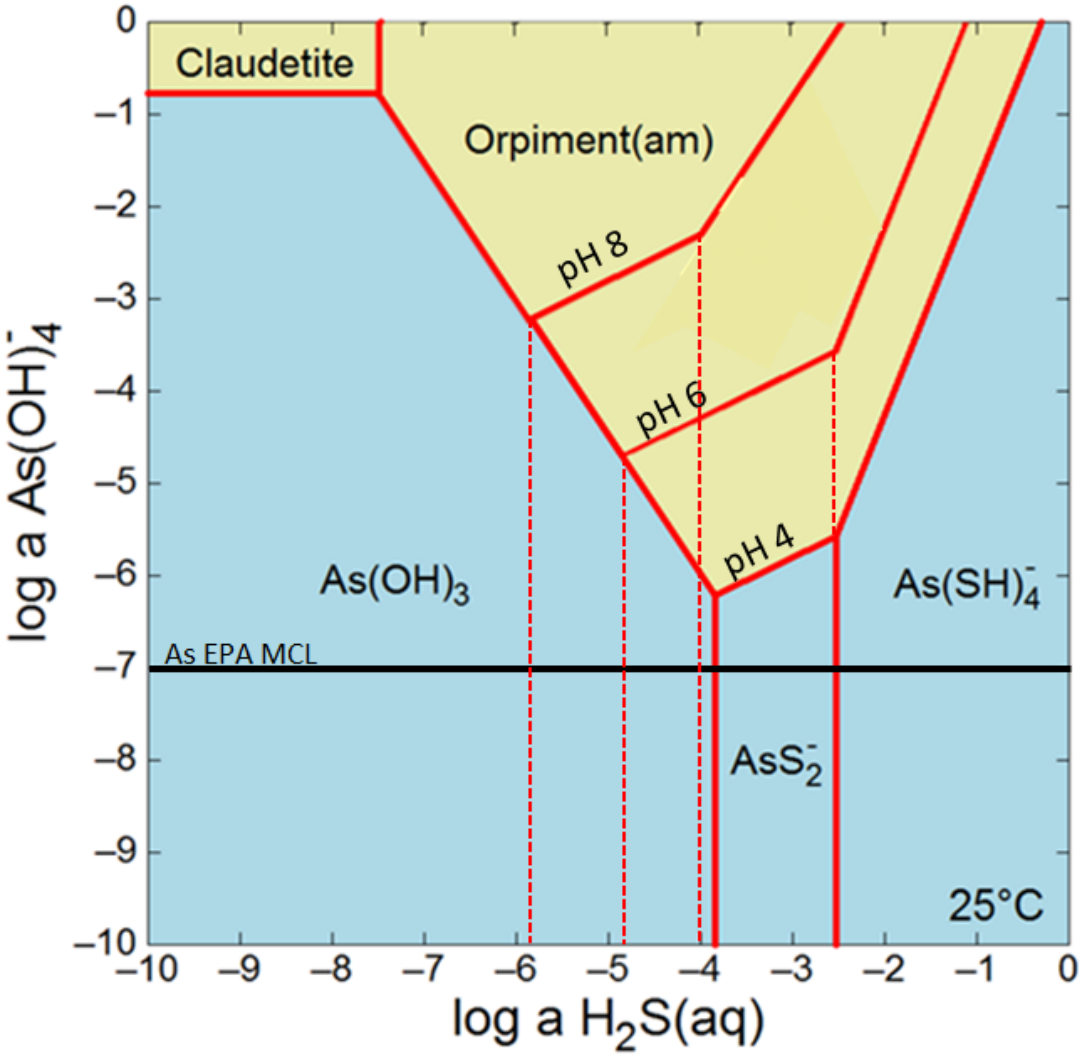

Figure 25. Activity-Activity diagram displaying the solubility of amorphous orpiment at varying pH and H_2S conditions.

The next set of reactions were modeled using GWB's React program (Bethke, 2008). This modeling program calculates relationships of aqueous species present in the system (specifically designed for the field site) at varying conditions to allow predictions of several significant geochemical interactions specific to the system. The purpose of these reaction path models in this study was to predict changes in dominant mineralogy (moles of minerals precipitated out of the groundwater) and arsenic concentrations under sliding Eh conditions, before and after the addition of $FeSO_4$ to the aquifer at the site-specific conditions. GWB like all quantitative models contain limitations. The thermodynamic data used in these models were calculated in a lab setting at varying temperatures depending on the phase (aqueous species-low temperature, mineral solubilities-high temperature) thus are prone to inaccuracy and vary in quality (Bethke, 1996). This usually results in a lower resolution model as compared to the extreme complexity of the reactions that occur in natural systems. This is especially true for this set of models as the thermodynamic data is limited to 1 wt. % arsenic arsenian-pyrite as determined by Saunders et al. (2008). As shown by the EMP data above the amount arsenic that is sequestered into the pyrite grains vary and thus thermodynamic data is needed for arsenian-pyrite with varying arsenic contents to create a more refined model for this system.

The pre-injection groundwater geochemistry of well I-1 was used to set the initial condition for the simulations. Table 2 shows the observed changes in arsenic content and water chemistry over the one-year monitoring period. The initial groundwater contains about 190 ug/L of dissolved arsenic. The GWB model traces the mineralogical reactions and water chemistry changes as the Eh values slide from +0.15 V to -0.15 V. The predicted mineralogical changes are shown in Figure 26. As the system transitions from oxidizing to reducing conditions there is a

shift in dominant mineralogy from hematite to arsenian-pyrite at an Eh of -.05 V. The arsenian-pyrite forms by the following reactions:

$$SO_4^{2-} + 2CH_2O + 2H^+ \longrightarrow H_2S + H_2CO_3$$

$$Fe^{2+} + 1.995\ H_2S + 0.01\ As(OH)_4^- + 2\ H^+ \longrightarrow FeS_{1.99}As_{0.01} + 1.02\ H_2O + 3.5\ O_2(aq)$$

This precipitation of about 10^{-5} mol of arsenian-pyrite in 1 kg solution results in only about 12 ug/L decrease in the dissolved arsenic concentration (from 190 to 178 ug/L) in the groundwater at the end of reaction path (Figure 27). These results demonstrate that the precipitation of arsenian-pyrite in response to a decreasing Eh would not lower arsenic concentrations below the EPA's MCL of 10 ug/L, thus an amendment of $FeSO_4$ is required to increase the amount of pyrite precipitation and arsenic sequestration.

The second reaction path model (Figures 28 and 29) was created to predict how much $FeSO_4$ would need to be added to this system to form enough arsenian-pyrite to drive the arsenic concentration below the EPA limit of 10 ug/L. This model traces the mineralogical reactions and water chemistry changes as 2.47 mmol of $FeSO_4$ was added into 1 kg of initial I-1 groundwater and Eh values slide from 0.5 V to -0.2 V. In this simulation, the more thermodynamic stable hematite phase is replaced by amorphous $Fe(OH)_3$ in the initial system. The amendments of $FeSO_4$ would increase the concentrations of Fe^{2+} and SO_4^{2-} in the ground water from 0.47 mg/L and 16 mg/L (pre-injection groundwater concentrations) to 40 mg/L and 60 mg/L respectively. The modeling results show that much more (10^{-4} mol) arsenian-pyrite forms per kg of groundwater as compared to the case without amendments (Figures 26 and 27). The groundwater arsenic concentration drops significantly from 190 ug/L to below the EPA's MCL of 10 ug/L. This modeling results indicate that $FeSO_4$ amendments is necessary to sequester arsenic below

EPA's MCL at the site investigated, which is consistent with the field results. The geochemical modeling techniques can help quantify the $FeSO_4$ amendments required to sequester arsenic below EPA's MCL. The dominant mineralogy shifts from an iron oxy-hydroxide ($Fe(OH)_3$) at more oxidizing environments (0.5-0.2 V) to the formation of arsenian-pyrite at increasingly reducing conditions (-0.02 to -0.2V) with the reappearance of the $Fe(OH)_3$ at more reducing conditions (<-0.17 V) as more Fe is amended into the system.

Table 2. Chemical conditions and major ion concentrations (mg/L) vs. time of groundwater samples for well I-1

Date	pH	Eh	Fe^{2+}	SO_4	H_2S	As	Cl	Na	K	Ca	Mg
2/15/2016 (Pre-injection)	6.24	125.7	0.47	16.0	0.044	0.19	8.0	3.939	0.262	25.16	1.904
2/24/2016 (Weekly event 1)	8.00	-142.1	53.80	800.0	6.020	3.80	180.0	15.39	318.3	78.22	28.55
3/2/2016 (Weekly event 2)	4.78	-37.0	138.5	330.0	0.350	13.00	110.0	11.38	183.3	68.24	18.56
3/9/2016 (Weekly event 3)	4.73	-22.1	40.50	34.0	0.550	6.50	39.0	6.378	68.84	34.98	7.535
3/17/2016 (Weekly event 4)	5.48	1.0	2.96	13.0	0.270	4.00	21.0	3.134	20.44	29.21	3.978
4/21/2016 (Monthly event 1)	6.07	-26.0	4.80	1.4	0.250	1.40	11.0	2.293	1.565	19.01	1.507
5/19/2016 (Monthly event 2)	6.13	-29.1	3.20	1.4	0.022	0.66	8.5	2.644	0.967	27.74	2.351
6/15/2016 (Monthly event 3)	6.29	-104.7	2.70	32.0	0.687	0.30	5.1	2.718	0.634	24.49	1.905
7/20/2016 (Monthly event 4)	6.26	-145.4	1.90	67.0	1.750	0.28	3.5	1.927	0.480	48.68	3.218
8/17/2016 (Monthly event 5)	5.29	-8.8	2.50	53.0	0.440	0.48	2.8	2.080	0.421	13.02	1.275
9/21/2016 (Monthly event 6)	6.07	-57.7	2.00	14.0	0.250	0.61	3.8	1.847	0.254	17.78	1.423
10/26/2016 (Monthly event 7)	6.37	-38.0	1.80	29.0	0.070	0.40	3.3	1.612	0.296	51.90	3.302
11/15/2016 (Monthly event 8)	6.30	-40.9	2.30	56.0	0.110	1.10	4.6	1.817	0.528	54.30	3.236
12/13/2016 (Monthly event 9)	5.58	22.7	1.30	86.0	0.030	0.33	3.9	1.897	0.395	42.18	2.338
1/25/2017 (Monthly event 10)	3.16	455.7	1.72	140.0	0.010	0.07	4.0	1.410	0.178	25.23	1.788
2/15/2017 (Monthly event 11)	3.46	342.2	1.08	49.0	0.050	0.19	3.9	1.249	0.149	14.96	0.875

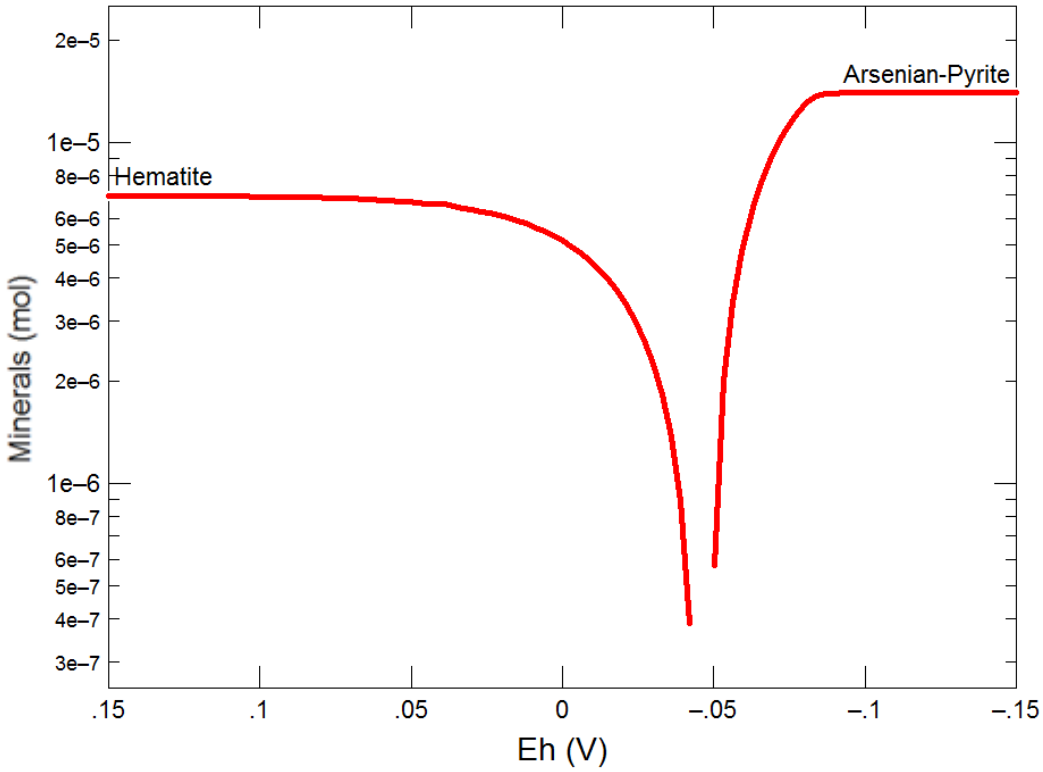

Figure 26. Geochemist's Workbench reaction path model showing the dominant mineralogy and the corresponding amount of moles of the precipitate under shifting redox conditions using the groundwater composition of the industrial site pre-injection.

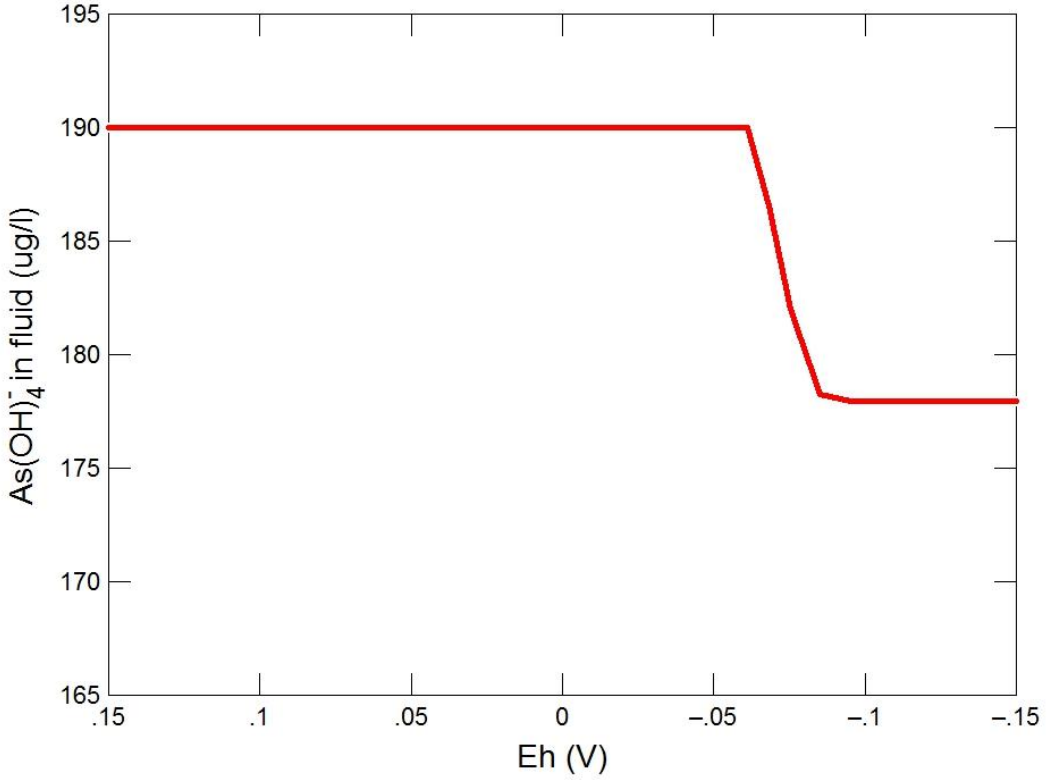

Figure 27. Plot showing the arsenic groundwater concentration through shifting Eh conditions using pre-injection groundwater composition.

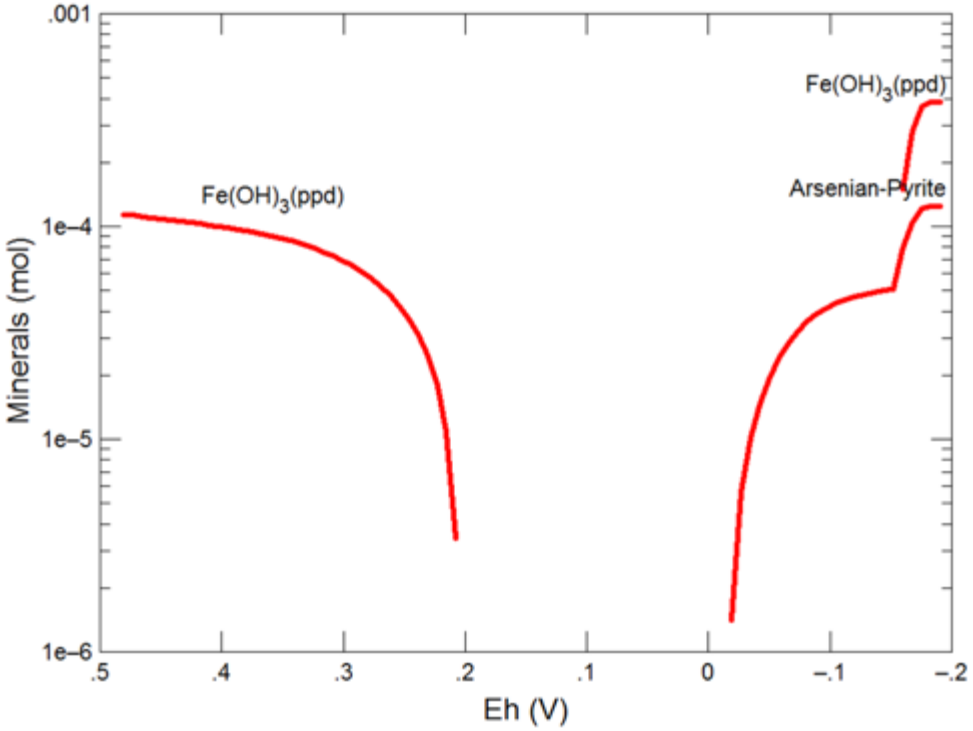

Figure 28. Geochemist's Workbench reaction path model showing the mineralogy under conditions with iron and sulfate concentrations great enough to drop the arsenic groundwater concentration below the EPA limit.

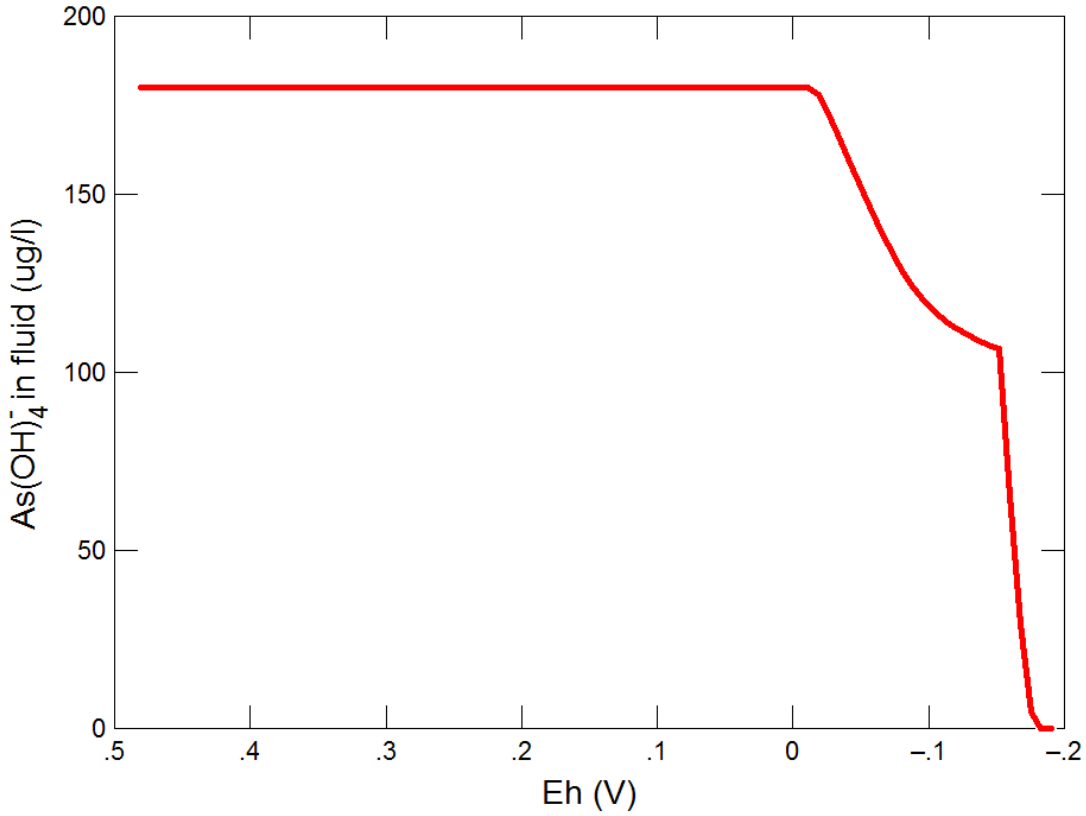

Figure 29. Plot showing arsenic groundwater concentrations through shifting Eh conditions using a groundwater composition with elevated levels of iron and sulfate.

Comparison to Similar Studies

The data presented in this study demonstrates that indigenous SRB in an arsenic contaminated aquifer with slightly reducing conditions can be stimulated by the injection of an added amendment (organic carbon, $FeSO_4$, and fertilizer) to the point of catalyzing sulfate reduction. These conditions led to the formation of arsenian-pyrite and the subsequent decrease in the concentration of arsenic in the groundwater below the sites regulatory limit for a duration of six months. Other lab and field studies have examined similar methods of remediation through the formation of biogenically precipitated iron sulfide minerals. Lab experiments such as Onstott et al. (2011), set up columns containing ground water and sediments sampled from an arsenic contaminated site. These columns were then brought under sulfate reducing conditions which resulted in a decrease of the dissolved arsenic concentration through the precipitation of biogenic iron sulfide minerals.

Pi et al. (2017), the only other field study that was designed to remove arsenic from a contaminated aquifer through the stimulation of SRB and subsequent precipitation of iron sulfide minerals had success with decreasing the overall concentration of arsenic in the aquifer from 593 µg/L to 136 µg/L (77% removal rate). Their short term (55 day) study involved periodic injections of $FeSO_4$ and anoxic water to facilitate a shift to more sulfate reducing conditions and activating in-situ SRB. XRD results confirmed that several iron sulfide minerals formed including mackinawite, arsenopyrite, and pyrite, with mackinawite constituting the predominate iron sulfide mineral formed. When comparing the Pi et al. (2017) study with the study documented in this thesis there are some distinct difference that need to be pointed out. Firstly, the addition of organic carbon in the injection solution in this study provided SRB with electrons that aided in the reduction of sulfate into hydrogen sulfide. Perhaps the higher concentration of

hydrogen sulfide in the ground water led to greater precipitation rates of iron sulfides minerals leading to a higher arsenic removal rate, which is observed in this study to be >90 %. The XRD results of this study, confirmed the formation of only one iron sulfide mineral (aresnian-pyrite) as compared to serval iron sulfide minerals in the Pi et al. (2017) study. No mackinawite was observed in this study indicating that the arsenian-pyrite was either directly precipitated from the ground water and/or mackinwate formed intermediately to the arsenian-pyrite within the first week post injection before the first sampling period.

Conclusions

This study, representing one of the first long-term (yearlong) studies of its kind, successfully demonstrated that through the biologically induced formation of arsenian-pyrite, arsenic could effectively be sequestered at levels high enough to bring the concentration in the groundwater below this industrial sites regulatory limit. The remediation strategy employed at this field site was specialized to site-specific factors such as ORP, pH, and dominant groundwater composition. Further successful implementation of this bioremediation technique will need to be mindful to variations in these site-specific factors to achieve similar results. The main conclusions of this study are listed below:

- Approximately one week after the injection the sulfate reducing conditions were established in the groundwater as observed by low ORP and high H_2S level. This shift to sulfate reducing conditions led to a significant decrease in the arsenic concentration (below the sites regulatory limit) as arsenian-pyrite began to precipitate out of the groundwater. Sulfur isotope data concluded these chemical changes were associated with the activation of SRB.

- XRD, XRF, and EMP analyses all provided data that confirmed that soluble arsenic in the groundwater was being sequestered into arsenian-pyrite in amounts that ranged between 0.05 to 0.4 wt. % arsenic; indicating arsenian-pyrites capacity to sequester arsenic when quickly precipitated from solution.
- The SEM anaylsis revealed the arsenian-pyrite grew to form well-formed euhedral crystals (1 to 10 µm in diameter) or spherical aggregates (10 to 50 µm in diameter).
- The main sequestration stage, with total arsenic removal rates >90%, lasted for at least six months until the arrival of untreated groundwater from up-gradient. Of the total arsenic removal rate, co-precipitation and sorption processes accounted for >80%.
- Geochemical modeling showed the sequestration capacity of another arsenic sulfide mineral (amorphous orpiment) was unable to remove arsenic at concentrations low enough to comply with the EPA's drinking water standards. Further modeling using site specific conditions demonstrated that an added amendment of $FeSO_4$ is needed to supply the SRB with enough iron and sulfate to form pyrite at great enough levels to sequester arsenic below the regulatory limit.
- For a full-scale remediation, the biostimulation should start at positions hydrologically up-gradient from the major plume, aquifers may need repeated amendment with organic carbon to re-establish the reducing conditions that favor arsenic sequestration.
- Further full scale research still needs to be conducted to assess the effectiveness of this remediation technique over larger distance scale. Research also needs to be conducted to test the long-term stability of arsenian-pyrite as an effective sink for arsenic.

Overall, this study has demonstrated the effectiveness of this cheap and environmentally friendly bioremediation method at the field scale. This study helps refine this field bioremediation technique using indigenous SRB, which could be adapted from industrial cleanups to provide clean drinking water to the millions of people around the world that are effected by arsenic groundwater contamination.

References

Aziz, Z., Bostick, B.C., Zheng, Y., Huq, M.R., Rahman, M.M., Ahmed, K.M., van Geen, A., 2016. Evidence of decoupling between arsenic and phosphate in shallow groundwater of Bangladesh and potential implications: Applied Geochemistry, 30, 1-11.

Beale A.M., Jacques S.D.M., Weckhuysen B.M., 2010. Chemical imaging of catalytic solids with synchrotron radiation: Chemical Society Review, 39, 4656-4672.

Bethke, C.M.. 1996. Geochemical Reaction Modeling; Oxford University Press: New York.

Bethke, C. M., 2008. Geochemical and biogeochemical reaction modeling, Cambridge University Press, 543 pp.

Bish, D.L., Post, J.E., 1989. Modern Powder Diffraction. Reviews in Mineralogy: Mineralogical Society of America, 20, 220-231.

Bostick, B.C., Fendorf, S., 2003. Arsenic sorption on troilite (FeS) and pyrite (FeS_2): Geochimica Cosmochimica Acta, 67, 909-921.

Bulut, G. .B.C., Yenial, Ü., Emiroğlu, E., Sirkeci, A.A., 2014. Arsenic removal from aqueous solution using pyrite: Journal of Cleaner Production, 84, 526–532.

Chapelle, F. H., Lovley, D.R., 1992. Competitive exclusion of sulfate reduction by Fe(III) reducing bacteria: A mechanism for producing discrete zones of high-iron groundwater: Ground Water, 30, 29-36.

Couture, R.-M., Rose, J., Kumar, N., Mitchell, K., Wallschlager, D., Van Cappellen, P., 2013. Sorption of arsenite, arsenate and thioarsenates to iron oxides and iron sulfides: A kinetic and spectroscopic investigation: Environmental Science and Technology, 47, 5652-5659.

DeFlaun, M., Lanzon, J., Lodato, M., Henry, S., Onstott, T. E., Chan, E., Otemuyiwa, B., 2009. Anaerobic Biostimulation for the In Situ Precipitation and Long-Term Sequestration of Metal Sulfides. Technical Report DTIC Document.

Fitton, G., 1997. X-Ray fluorescence spectrometry, in Gill, R. (ed.), Modern Analytical Geochemistry: An Introduction to Quantitative Chemical Analysis for Earth, Environmental and Material Scientists. Addison Wesley Longman, UK.

Fitzsimons, I.C.W., Harte, B., Clark, R.M., 2000. SIMS stable isotope measurement: counting statistics and analytical precision: Mineral, 64**,** 59-83.

Ford, R.G., Wilkin, R.T., Puls, R.W., 2007. Monitored Natural Attenuation of Inorganic Contaminants**:** Groundwater, 2, 104-108.

Gartman, A., Luther., G. W., 2013. Comparison of pyrite (FeS2) synthesis mechanisms to reproduce natural FeS2 nanoparticles found at hydrothermal vents**:** Geochimica Cosmochimica Acta, 120, 447–458.

Ghandehari, S, 2016. Bioremediation of an Arsenic-Contaminated Site, Using Sulfate Reducing Bacteria, Bay County, Florida. Master's Thesis, Auburn University. 115 p.

Han D.S., Song J.K., Batchelor B., Abdel-Wahab A., 2013. Removal of arsenite (As(III)) and arsenate(As(V)) by synthetic pyrite (FeS_2): Synthesis, effect of contact time, and sorption/desorption envelopes: Journal of Colloid and Interface Science, 392, 311-318.

Hounslow, A.W., 1980. Groundwater Geochemistry: Arsenic in Landfills: Ground Water, 18, 331-333.

Huerta-Diaz, M.A., J.W. Morse., 1992. Pyritization of trace metals in anoxic marine sediments: Geochimica Cosmochimica Acta, 56**,** 2681-2702.

Jingtai, H., Fyfe, W.S., 2000. Arsenic removal from water by iron-sulphide minerals: Chinese Science Bulletin, 45, 1430-1434.

Kinniburgh D. G., Smedley P. L., 2001. Arsenic Contamination of Groundwater in Bangladesh (British Geologic Survey Report, 2001)

Le Pape P., Blanchard M., Brest, J., Boulliard, J-C., Ikogou M., Stetten L., Wang S., Landrot G., Morin G., 2017. Arsenic incorporation in pyrite at Ambient temperature at Both tetrahedral S^{-1} and Octahedral Fe^{II} sites: Evidence from EXAFS-DFT Analysis: Environmental Science Technology, 51, 150-158.

Lee, M. K., Saunders J.A., Harrington J., Lutes C., Wilkin R., 2008. Strategy for in situ bioremediation of arsenic in groundwater: Field and modeling studies: Remediation of Recalcitrant Contaminants.

Lee, M.-K., Saunders, J. A., 2003. Effects of pH on metals precipitation and sorption: Field bioremediation and geochemical modeling approaches: Vadose Zone Journal, 2, 177-185.

Lee, M.-K., Saunders, J. A., Wolf, L. W., 2000. Effects of geologic heterogeneities on pump-and-treat and in-situ bioremediation: A stochastic analysis: Environmental Engineering Science, 17, 183-189.

Lee, M.-K., Saunders, J.A., Wilkin, R.T., Mohammad, S., 2005. Geochemical modeling of arsenic speciation and mobilization: Implications for bioremediation, in Advances in Arsenic

Research: Integration of Experimental and Observational Studies and Implications for Mitigation: American Chemical Society Symposium Series, 915, 398-413.

Levitt, L., Ghandehari, S., Lee, M.-K., Saunders, J. A., 2016. Field-scale Bioremediation of Arsenic-Contaminated Groundwater Using Sulfate Reducing Bacteria: Geochemical Monitoring and Hydrological Modeling. Geological Society of America Poster Abstract.

Mandal, B.K., Suzuki, K.T., 2002. Arsenic Round the World: A Review: Talanta, 58, 201-235.

Mintz, J., Miller, J., 1993. Lynn Haven Retired Substation Remedial Action Plan: Southern Company Services, 196 p.

Neumann, R.B., Ashfaque, K.N., Badruzzaman, A.B.M., Ali, A., Shoemaker, J.K., Harvey, C.F., 2010. Anthropogenic influences on groundwater arsenic concentrations in Bangladesh: Nature Geoscience, 3, 46-52.

Nordstrom, D. K., 2002. Worldwide occurrences of arsenic in groundwater: Science, 296, 2143-2145.

Onstott, T.C., Chan, E.; Polizzotto M.L., Lanzon, J., DeFlaun, M.F., 2011. Precipitation of arsenic under sulfate reducing conditions and subsequent leaching under aerobic conditions: Applied Geochemistry, 26, 269-285.

Pi, K., Wang, Y., Xie, X., Ma, T., Liu, Y., Su, C., Zhu, Y., Wang, Z., 2017. Remediation of arsenic-contaminated groundwater by in-situ stimulating biogenic precipitation of iron sulfides: Water Research, 109, 337-346.

Reed, S. J. B., 2005. Electron Microprobe Analysis and Scanning Electron Microscopy in Geology (2nd Ed.), Cambridge University Press.

Rieder M., Crelling J.C., Šustai O., Drábek M., Weiss Z., Klementová, M., 2007. Arsenic in iron disulfides in a brown coal from the North Bohemian Basin, Czech Republic.International: Journal of Coal Geology, 71, 115-121.

Saunders J. A., Pritchett M. A., Cook R. B., 1997. Geochemistry of biogenic pyrite and ferromanganese coatings from a small watershed: A bacterial connection?: Geomicrobiology Journal, 14, 203–217.

Saunders J. A., Lee M.-K., Uddin A., Mohammad S., Wilkin R., Fayek M., Korte N., 2005a. Natural arsenic contamination of Holocene alluvial aquifers by linked tectonic, weathering, and microbial processes: Geochemistry, Geophysics, Geosystems, 6**,** 66-81.

Saunders J. A., Lee M.-K., Wolf L., Morton C., Feng Y., Thomson I., Park S., 2005b. Geochemical, Microbiological, and Geophysical Assessments of Anaerobic Immobilization of Heavy Metals: Bioremediation Journal, 9, 33–48.

Saunders, J., Lee, M.-K., Shamsudduha, M., Dhakal, P., Uddin, A., Chowdury, M., Ahmed, K., 2008. Geochemistry and mineralogy of arsenic in (natural) anaerobic groundwaters: Applied Geochemistry, 23, 3205–3214.

Schoonen, M.A.A., Barnes, H.L., 1991. Reactions forming pyrite and marcasite from solution: II. Via FeS precursors below 100 C: Geochimica Cosmochimica Acta, 55, 1505-1514.

Schmidt, W., Clark, M. W., 1980. Geology of Bay County, Florida. 57. Bureau of Geology, Division of Resource Management, Florida Department of Natural Resources.

Smedley, P., Kinniburgh, D., 2002. A review of the source, behaviour and distribution of arsenic in natural waters: Applied Geochemistry, 17, 517–568.

Schweitzer, P., 2017. Florida geologic map data. Interactive maps and downloadable data for regional and global geology, geochemistry, geophysics, and mineral resources; products

of the USGS Mineral Resources Program. Available at: https://mrdata.usgs.gov/geology/state/state.php?state=FL [Accessed March 22, 2017].

Starnes P., 2015. Hydrogeology and Geochemistry of Arsenic Contaminated Shallow Alluvial Aquifers in Florida and Alabama. Master's Thesis, Auburn University. 134p.

Thode, H.G., Kleerekoper, H., McElcheran, E., 1951. Isotope fractionation in the bacteria reduction of sulfate: Research (London), 4, 581-582.

USEPA, 1997. Technology alternatives for the remediation of soils contaminated with As, Cd, Cr, Hg, and Pb, , Washington DC: Office of Emergency and Remedial Response, U.S. Environmental Protection Agency. EPA/540/S-97/500 45p.

USEPA, 2001. Drinking Water Standard for Arsenic , Washington DC: Office of Water, U.S. Environmental Protection Agency. EPA 815-F-00-015. 78 p.

USEPA, 2002. Proven alternatives of aboveground treatment of arsenic in groundwater: Washington DC, Office of Solid Waste and Emergency Response, U.S. Environmental Protection Agency, EPA-542-S-02-002, 68 p.

Webster, J. G., 1990. The solubility of As_2S_3 and speciation of As in dilute and sulphide-bearing fluids at 25 and 90 C: Geochimica Cosmochimica Acta, 54, 1009–1017.

Wilkin, R.T., Barnes, H.L., 1996. Pyrite formation by reactions of iron monosulfides with dissolved inorganic and organic sulfur species: Geochimica Cosmochimica Acta, 60, 4167-4179.

Wilkin R.T., Wallschlager D., Ford R.G., 2003. Speciation of arsenic in sulfidic waters: Geochemical Transactions, 4, 1-7.

Wolthers M., Charlet L., Van Der Linde P.R., Rickard D., 2005. Arsenic mobility in the ambient sulfidic environment: Sorption of arsenic(V) and arsenic(III) onto disordered mackinawite: Geochimica Cosmochimica Acta, 69, 3483-3492.

Woolson, E.A., 1983. in: W.H. Lederer, R.J. Fensterheim, Industrial, Biomedical and Environmental Perspective, Van Nostrand Reinhold Company, New York, 393.

Zouboulis, A.I., Kydros, K.A., Matis, K.A., 1993. Arsenic(III) and Arsenic(V) removal from solutions by pyrite fines: Separation Science and Technology, 28, 2449–2463.